Biomaterials 34 (2013) 492–500

Contents lists available at SciVerse ScienceDirect

Biomaterials

journal homepage: www.elsevier.com/locate/biomaterials

Gd-DTPA-loaded polymer–metal complex micelles with high relaxivity for MR cancer imaging

Peng Mi [a], Horacio Cabral [a], Daisuke Kokuryo [b], Mohammad Rafi [c], Yasuko Terada [d], Ichio Aoki [b], Tsuneo Saga [b], Ishii Takehiko [a], Nobuhiro Nishiyama [c,**], Kazunori Kataoka [a,c,e,*]

[a] Department of Bioengineering, Graduate School of Engineering, The University of Tokyo, 7-3-1 Hongo, Bunkyo-ku, Tokyo 113-8656, Japan
[b] Molecular Imaging Center, National Institute of Radiological Sciences, Anagawa 4-9-1, Inage, Chiba 263-8555, Japan
[c] Center for Disease Biology and Integrative Medicine, Graduate School of Medicine, The University of Tokyo, 7-3-1 Hongo, Bunkyo-ku, Tokyo 113-0033, Japan
[d] SPring 8, JASRI, 1-1-1 Kouto, Sayo-cho, Sayo-gun, Hyogo 679-5198, Japan
[e] Department of Materials Engineering, Graduate School of Engineering, The University of Tokyo, 7-3-1 Hongo, Bunkyo-ku, Tokyo 113-8656, Japan

ARTICLE INFO

Article history:
Received 12 July 2012
Accepted 16 September 2012
Available online 8 October 2012

Keywords:
Micelles
Drug delivery
Magnetic resonance imaging (MRI)
Polymer-metal complex
Cancer diagnosis

ABSTRACT

Nanodevices for magnetic resonance imaging of cancer were self-assembled to core–shell micellar structures by metal complex formation of K_2PtCl_6 with diethylenetriaminepentaacetic acid gadolinium (III) dihydrogen (Gd-DTPA), a T_1-contrast agent, and poly(ethylene glycol)-*b*-poly{N-[N′-(2-aminoethyl)-2-aminoethyl]aspartamide} (PEG-*b*-PAsp(DET)) copolymer in aqueous solution. Gd-DTPA-loaded polymeric micelles (Gd-DTPA/m) showed a hydrodynamic diameter of 45 nm and a core size of 22 nm. Confining Gd-DTPA inside the core of the micelles increased the relaxivity of Gd-DTPA more than 13 times (48 mM^{-1} s^{-1}). In physiological conditions Gd-DTPA/m sustainedly released Gd-DTPA, while the Pt(IV) complexes remain bound to the polymer. Gd-DTPA/m extended the circulation time in plasma and augmented the tumor accumulation of Gd-DTPA leading to successful contrast enhancement of solid tumors. μ-Synchrotron radiation-X-ray fluorescence results confirmed that Gd-DTPA was delivered to the tumor site by the micelles. Our study provides a facile strategy for incorporating contrast agents, dyes and bioactive molecules into nanodevices for developing safe and efficient drug carriers for clinical application.

1. Introduction

Early detection of neoplastic lesions is critical for success in cancer therapy. Magnetic resonance imaging (MRI) provides a powerful diagnostic imaging modality of cancer, because of its non-invasiveness, high definition and precise three-dimensional positioning ability [1,2]. Paramagnetic compounds are widely used as MRI contrast agents (CAs) to amplify the signals of MRI tomography and improve the contrast between magnetic similar but histological dissimilar tissues [3,4]. Several low molecular weight paramagnetic complexes of gadolinium(III) are used for clinical MRI as they can decrease the longitudinal relaxation time T_1 of surrounding water protons [5–7]. Among these complexes, Gd-DTPA, one of the most commonly used T_1-contrast agent for clinical MRI, is featured by high thermodynamic and kinetic stabilities, which reduce the release of toxic Gd^{3+} ions, besides a longitudinal relaxivity, r_1, of ~3.5 mM^{-1} s^{-1} at 1.4 T [3,5,7]. Nevertheless, the inherent low relaxivity, short circulation time in blood and low specificity to tissues limit its applications. From this viewpoint, high relaxivity CAs with promoted tissue detection and hindered release of free Gd^{3+} ions are required to improve the performance of imaging.

Nanodevices have been recently developed to selectively deliver imaging agents to solid tumors by leaking out from circulation due to the enhanced permeability of the tumor vasculature [8–12]. In this way, macromolecules, liposomes, dendrimers and nanoparticles carrying high payloads of CAs have been developed to enhance the MR contrast of solid tumors [13–25]. In most cases, Gd-based CAs were covalently incorporated to the structures of nanocarriers to increase the bloodstream circulation, the tumor accumulation and, in some cases, the relaxivity of the loaded CAs

* Corresponding author. Department of Bioengineering, Graduate School of Engineering, The University of Tokyo, 7-3-1 Hongo, Bunkyo-ku, Tokyo 113-8656, Japan. Tel.: +81 3 5841 7138; fax: +81 3 5841 7139.
** Corresponding author. Tel./fax: +81 3 5841 1430.
E-mail addresses: nishiyama@bmw.t.u-tokyo.ac.jp (N. Nishiyama), kataoka@bmw.t.u-tokyo.ac.jp (K. Kataoka).

0142-9612/$ – see front matter © 2012 Elsevier Ltd. All rights reserved.
http://dx.doi.org/10.1016/j.biomaterials.2012.09.030

[14,22,23]. Nevertheless, covalent binding of Gd-chelates to macromolecular systems may increase the risk of Gd^{3+} ion leakage from the chelates due to the prolonged half-life in the body and cumulative toxicity [26]. Thus, the design of tumor-targeted nanodevices for Gd-based CAs should consider such issues for constructing safe carriers, which could target the tumor position and release Gd-DTPA easily from nanodevices.

Among promising nanodevice systems for MRI, block copolymeric micelles, i.e. nanostructures consisting of a drug-loaded core and poly(ethylene glycol) (PEG) protective shell, present exceptional advantages including their relatively small sizes, ability to engineer drug loading mechanisms, controlled release of their cargo, prolonged life in the bloodstream and enhanced accumulation in solid tumors after intravenous administration [19–25]. Auspicious results from clinical trials of micelle formulations incorporating anticancer agents indicate the potential clinical application of polymeric micelles [27,28].

The aim of this study was to develop core–shell type micellar nanocarriers of Gd-DTPA for tumor imaging, which can incorporate Gd-DTPA via the reversible Pt-Gd-DTPA complexation, allowing sustained release of free Gd-DTPA in biological environments. In order to incorporate hydrophilic low molecular weight paramagnetic complexes Gd-DTPA into polymeric micelle, we utilized Pt(IV) ions to "cross-link" carboxyl groups of Gd-DTPA to amino groups of PEG-*b*-PAsp(DET) copolymers. Gd-DTPA/m could passively accumulate in solid tumors due to the enhanced permeability and retention (EPR) effect. Thus, the improved tumor accumulation of Gd-DTPA could enhance the T_1 weighed contrast of the malignancies in mice. Otherwise, in physiological environments such as plasma, the ligand exchange reaction of Pt(IV) from the carboxylic group of Gd-DTPA to chloride ions results in sustained release of free Gd-DTPA, which can be rapidly cleared from the body via glomerular excretion.

2. Materials and methods

2.1. Materials

α-Benzyl-L-aspartate *N*-carboxy anhydride (BLA-NCA) was obtained from Chuo Kaseihin Co., Inc. (Tokyo, Japan). Poly(ethylene glycol) (MeO-PEG-NH_2) (M_w = 12,000, M_w/M_n = 1.03) were purchased Nippon Oil and Fats Co., Ltd. (Tokyo, Japan). Benzene, *N*,*N*-dimethylformamide (DMF), *n*-butylamine, dichloromethane (CH_2Cl_2), diethylenetriamine (DET), potassium hexachloroplatinate(IV) (K_2PtCl_6) and *N*-methyl-2-pyrrolidone (NMP) were purchased from Wako Pure Chemical Industries (Osaka, Japan) and distilled by a general method before use. Arsenazo III and Gd-DTPA were purchased from Aldrich Chemical (Milwaukee, USA), and then Gd-DTPA was converted to sodium salt by adjusting the pH to 7 with NaOH and lyophilization. 400-mesh copper grids were obtained from Nisshin E. M. Spectra/Por-6 membrane was purchased from Spectrum Laboratories (Rancho Dominguez, CA). Dulbecco's modified eagle's medium (DMEM) was obtained from Sigma–Aldrich Co. (St. Louis, USA). Fetal bovine serum (FBS) was purchased from MP Biomedicals, Inc. (Illkirch, France). 96-well culture plates were purchased from Becton Dickinson Labware (Franklin Lakes, USA). The Cell Counting Kit-8 was purchased from Dojindo Laboratories (Kumamoto, Japan).

Murine colon adenocarcinoma 26 (C-26) cells were kindly supplied by the National Cancer Center (Tokyo, Japan). Human umbilical vein endothelial cells (HUVEC), and the endothelial cell growth medium-2 bullet kit (EGM-2 bullet kit) were obtained from Lonza Ltd. (Basel, Switzerland). B16-F10 melanoma cells were purchased from the American Type Culture Collection (Virginia, USA). All the cells are maintained with medium in a humidified atmosphere containing 5% CO_2 at 37 °C. CDF_1 mice (female; 18–20 g body weight; 6 weeks old) were purchased from Charles River Japan (Kanagawa, Japan) and, treated following the policies of the Animal Ethics Committee of the University of Tokyo.

2.2. Synthesis of PEG-b-PAsp(DET)

As shown in Scheme S1, poly(ethylene glycol)-*b*-poly(β-benzyl L-aspartate) (PEG-*b*-PBLA) with different degree of polymerization (DP) (DP = 25, 35, 45) were synthesized by ring-opening polymerization of BLA-NCA initiated by MeO-PEG-NH_2 (M_w = 12,000) according to previously reported method with minor modification [29]. Briefly, BLA-NCA (1.1 g, 4.5 mmol) was dissolved in DMF (2 mL) and then diluted with CH_2Cl_2 (20 mL). MeO-PEG-NH_2 (1.2 g, 0.1 mmol) dissolved in CH_2Cl_2 was added to the solution of BLA-NCA. The reaction was carried out with stirring for 2 days at 35 °C. All the procedures above were under dry argon protection. PEG-*b*-PBLA was collected by precipitating in excess amount of diethyl ether, filtration and vacuumed to dry. In Figure S1, the ^1H NMR spectrum of PEG-*b*-PBLA was measured in d_6-DMSO at 80 °C with a JEOL EX300 spectrometer (JEOL, Tokyo, Japan) using tetramethylsilane (TMS) as an internal standard, and the degree of polymerization (DP = 25, 35, 45) was calculated from the peak intensity ratio of protons both in phenyl groups of PBLA ($C_6H_5CH_2$–, δ = 7.3 ppm) and methylene units (–CH_2CH_2–, δ = 3.6 ppm) of PEG. The polydispersity of PEG-*b*-PBLA was characterized by gel permeation chromatography (GPC) system (HLC-8220, TOSOH Co., Japan) equipped with TSK-gel columns (TOSOH Co., Tokyo, Japan) and an internal refractive index (RI) detector at 40 °C. NMP containing 50 mM LiBr was used as mobile phase with a flow rate of 0.35 mL/min and linear PEG standards were used for calibration. As shown in Figure S2, the GPC chromatogram of the prepared PEG-*b*-PBLA has a unimodal molecular weight distribution (M_w/M_n: 1.03).

PEG-*b*-PAsp(DET) with different DP (25, 35, 45) were prepared separately via aminolysis reaction of PEG-*b*-PBLA with DET following the protocol modified from our former reported method [30]. Briefly, lyophilized PEG-*b*-PBLA (200 mg, 0.01 mmol) was dissolved in NMP (2 mL) and maintained at 5 °C. DET (2.3 mL, 50-equivalent to BLA) was diluted with NMP (2.3 mL) and kept at 5 °C. PEG-*b*-PBLA was added to DET solution and reacted with stirring at 5 °C for 1 h. The reacted mixture was neutralized by 5 M HCl aqueous solution (13 mL, equivalent to the added amino groups) in an ice bath, then dialysis (MWCO: 6000–8000) against 0.01 M HCl aqueous solution, then dialyzed with Milli-Q water under 4 °C. PEG-*b*-PAsp(DET) as the chloride salt form was collected via freeze-dry of final solution. ^1H NMR (D_2O) measurement showed the disappearance of signals belonging to the benzyl group and all the signals featured with PEG-*b*-PAsp(DET) (Figure S3). Degree of polymerization (DP = 25, 35, 45) was calculated by comparing the peak intensity ratio between methylene protons of the α, β-Asp segment (peak f, δ = 2.8 ppm) and methylene units (–CH_2CH_2–, δ = 3.6 ppm) of PEG. GPC measurements of block copolymers were carried out utilizing a HPLC system (JASCO, Japan) equipped with Superdex 75 10/300 GL column (GE Healthcare UK, Ltd.) and UV detector set at 220 nm. The column was eluted with 10 mM AcOH buffer containing 500 mM NaCl (pH 7.4) at a flow rate of 0.5 mL/min at room temperature. The GPC chromatogram of the obtained PEG-*b*-PAsp(DET) was unimodal (Figure S4).

2.3. Preparation of Gd-DTPA-loaded micelles (Gd-DTPA/m)

K_2PtCl_6 (0, 1, 2.5, 5 and 10 mM) was dissolved in Milli-Q water adjusted to pH 7.4 using trace amount of NaOH or diluted in 5 mM PBS buffers, then mixed with Gd-DTPA (5 mM) to incubated at 37 °C for 24 h. PEG-*b*-PAsp(DET) (DP = 25, 35, 45; [DET] = 5 mM) was added to Pt/Gd-DTPA mixture ([Gd-DTPA]/[DET] = 1.0) and incubated at 4 °C for 120 h to spontaneously form Gd-DTPA loaded micelles (Gd-DTPA/m). The micelle was purified by dialysis (MWCO: 6000–8000) against Milli-Q water and ultrafiltration (MWCO: 30,000) to remove free drug and polymer in the solution. Size distribution of the Gd-DTPA/m was evaluated by dynamic light scattering (DLS) measurement at 25 °C using Zetasizer Nano ZS90 (Malvern Instruments, UK). The contents of platinum and gadolinium of micelles were determined by inductively coupled plasma-mass spectrometry (ICP-MS) (4500 ICP-MS; Hewlett Packard, USA).

2.4. Transmission electron microscopy (TEM)

The morphology of micelle was observed on a Transmission Electron Microscope (JEM-1400, JEOL, Japan) operated with 100 kv acceleration voltages and 40 uA beam current. Diluted micelle was stained by mixing with uranyl acetate solution (2%, w/v) and placed on 400-mesh copper grids. The diameters of the core of micelle and size distribution were calculated with Image J, which was designed and provided by National Institutes of Health (NIH). The elements distribution inside micelle was characterized using JEM-2100F (JEOL, Japan) under the scanning transmission electron microscopy (STEM) pattern and scanned by energy dispersive X-ray (EDX) spectra. The specimen for the elements measurements was prepared only loading micelle on 400-mesh copper grids without staining.

2.5. Arsenazo III colorimetric assay

Free Gd^{3+} was determined by the absorption of Gd-Arsenazo III complex referring one arsenazo III method [31]. Briefly, equal molar ratio of arsenazo III solution was mixed with of Gd-DTPA/K_2PtCl_6 mixtures, and then the absorbance spectra were measured using with an UV–vis spectrometer (V-570 UV/VIS/NIR Spectrophotometer, JASCO, Japan) at 660 nm. The absorbance of arsenazo III/$GdCl_3$, arsenazo III/Gd-DTPA, and arsenazo III were measured. All the solutions above were maintained at pH 7.4.

2.6. Release rate of Gd-DTPA from Gd-DTPA/m

The release characterization of Gd-DTPA from the micelle was evaluated by a dialysis method. 1 mL of Gd-DTPA/m solution and 1 mL PBS buffer (20 mM PBS with 300 mM NaCl) were put into dialysis bag (MWCO: 6000–8000) and

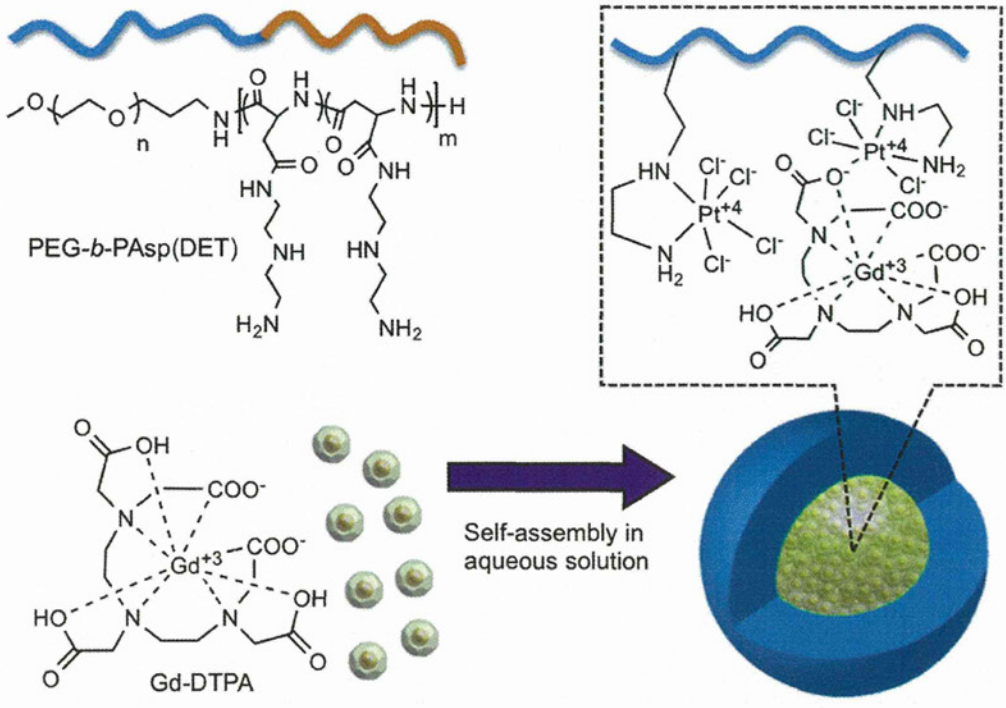

Scheme 1. Scheme illustration of the Gd-DTPA loaded micelle formation via polymer–metal complex formation.

incubated in 98 mL buffer of physiologic conditions (buffer: 10 mM PBS with 150 mM NaCl, temperature at 37 °C). 0.1 mL solution outside of the dialysis bag was sampled at defined time, and then the concentration of Gd-DTPA was measured by ICP-MS.

2.7. Characterization of r_1 relaxivity

The proton longitudinal relaxivity r_1, which is a parameter to evaluate the ability of contrast agents for MRI, can be determined from the change of the relaxation rate

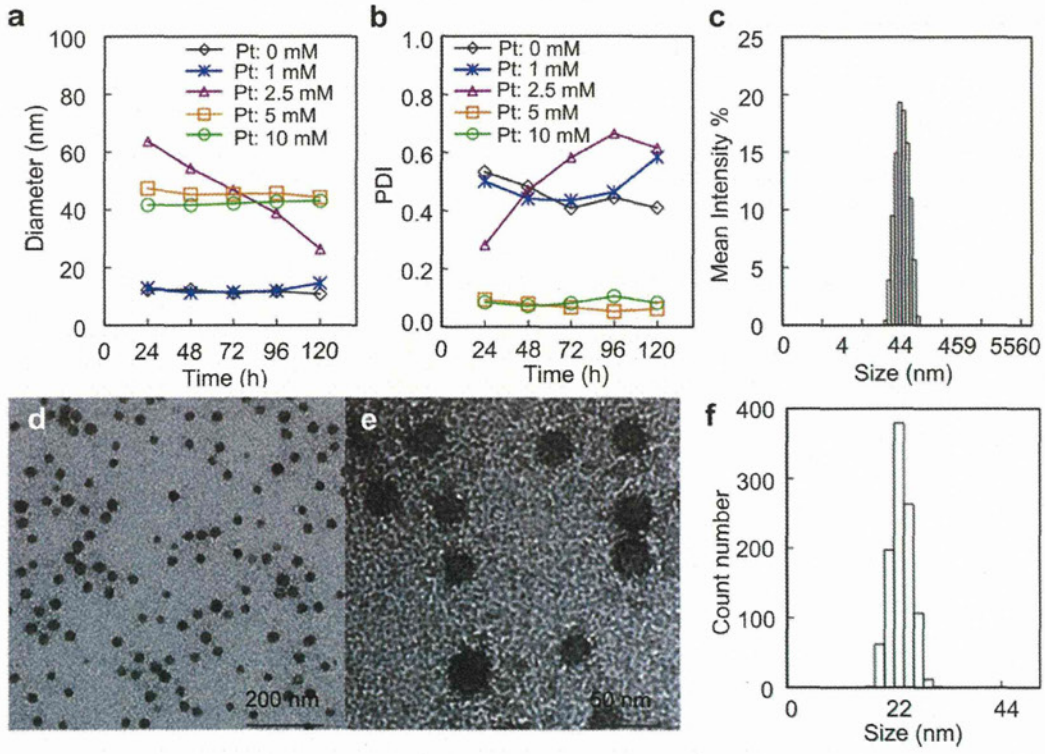

Fig. 1. Change in (a) average diameter and (b) polydispersity index (PDI) of Gd-DTPA/m with different Pt/Gd molar ratios, Gd-DTPA concentration was fixed at 5 mM, and Pt concentration ranged from 0 mM to 10 mM. (c) Size distribution measured by DLS. (d) and (e) TEM of Gd-DTPA/m. (f) Size distribution by number from TEM ($n = 1012$) calculated from Figure S6.

Table 1
Loading of Gd-DTPA/m prepared with different Pt/Gd ratio.

Sample (Pt:Gd-DTPA)	Pt linker loading	Gd-DTPA loading
0:5	0%	0%
1:5	~7.2%	~1.3%
2.5:5	~12.6%	~3%
5:5	~35%	~16%
10:5	~41%	~12%

Polymer PEG-*b*-PAsp (DET) 12k-45DP was used, the loading was calculated by dividing the drug amount to the total amount.

$1/T_1$ (s^{-1}) of water protons per mM concentration of CAs and calculated using expression $r_1 = (1/T_1 - 1/T_{1d})/[Gd]$, where $1/T_1$ is the longitudinal relaxation rate contrast in the presence of a paramagnetic species, $1/T_{1d}$ is the longitudinal relaxation rate contrast in the absence of a paramagnetic species and [Gd] is the concentration of paramagnetic CAs (mM). The T_1 values of Gd-DTPA, Gd-DTPA/m, or Gd-DTPA/K_2PtCl_6 solution of different Gd-DTPA/Pt ratios were measured at 37 °C in water or PBS buffer with a 0.59 T ^{1}H NMR analyzer (JNM-MU25A, JEOL) with a standard inversion-recovery pulse sequence.

2.8. Kinetic stability of Gd-DTPA/m

The stability of Gd-DTPA/m micelles under physiologic conditions was determined by DLS and static light scattering using Zetasizer Nano ZS90 (Malvern Instruments Ltd., UK). Changes of scattering light intensity were measured at defined time periods. A decrease in the scattering light intensity was associated with a decrease in the apparent molecular weight of the micelles and drug density inside the micelle core as well as in the micelle concentration. The size distribution and diameter of the Gd-DTPA/m were simultaneously monitored. The zeta-potential of Gd-DTPA/m was measured in phosphate buffer (10 mM) at pH 7.4 using Zetasizer Nano ZS90.

2.9. In vitro cytotoxicity evaluation

The cytotoxicity of Gd-DTPA/m against HUVEC and B16-F10 cell lines were evaluated by the CCK-8 assay. HUVEC and B16-F10 cells (5000 cells) were cultured with EGM-2 bullet kit and DMEM (containing 10% FBS), and then placed in 96-well plates, respectively. The cells were then exposed to Gd-DTPA, PEG-*b*-PAsp(DET), K_2PtCl_6 and Gd-DTPA/m for 72 h under 5% CO_2 at 37 °C. The Kit-8 solution was added, and followed by incubation under 5% CO_2 at 37 °C for 2.5 h. The absorbance at 450 nm of the produced WST-8 formazan in each well was measured using a using a micro-plate reader (Model 680, Bio-rad).

2.10. Cancer models

CDF_1 mice (female, 6 weeks old) were inoculated subcutaneously with C-26 cells (1×10^6 cells/mL). *In vivo* biodistribution, elemental mapping and MRI studies were performed when tumors were approximately 50 mm^3 in volume.

2.11. Biodistribution of Gd-DTPA/m

Gd-DTPA or Gd-DTPA/m was intravenously injected to the C-26 bearing mice at a dose of 78 μg/mouse on a Gd-DTPA basis. The mice were sacrificed after defined time periods (1, 4, 8 and 24 h). Tumors, livers, kidneys and spleens were excised. Blood was collected from the inferior vena cava, heparinized and centrifuged to obtain the upper plasma. Tissue samples were washed in PBS and weighed after removing excess fluid. The samples were dissolved in 90% HNO_3 and evaporated to dryness. The Pt and Gd concentrations were then measured by ICP-MS after the dried samples were dissolved in 1% HNO_3. The area under the curve (AUC) of a plot of liver, kidney, tumor and spleen drug concentration versus time was measured based on the trapezoidal rule up to 24 h after administration. Then, AUC ratios of tumor to liver, kidney and spleen are calculated.

2.12. Histology study

Mice bearing C-26 tumors were intravenously injected with Gd-DTPA/m at 100 μg/mouse on a Gd-DTPA basis. Twenty-four hours later, tumors were collected and immediately frozen in an acetone/dry ice mixture. The frozen samples were further sectioned at 6-μm thickness in a cryostat. Then, these thin sections were placed on glass slides, dehydrated in xylene and dehydrated with graded alcohols. These slides were stained with hematoxylin and eosin (H&E) and then samples were observed by using an AX80 microscope (Olympus, Japan).

2.13. In vivo MRI of Gd-DTPA/m

Solutions containing 0.2, 0.3, 0.4 and 0.5 mM Gd-DTPA or Gd-DTPA/m were placed in thin-wall PCR tubes, and then closed with flat caps for MR imaging at 1 T (Aspect, Aspect Imaging) and 7 T (BioSpec 70/20USR, Bruker). *In vivo* MR images were obtained using 1 T imaging spectrometer. For the T_1-weighted images of the mice, the following parameters were adopted: spin-echo method, repetition time (TR) = 400 ms, echo time (TE) = 11 ms, field of view (FOV) = 48 × 48 mm, matrix size = 256 × 256, and slice thickness = 2 mm. MR images were obtained from C-26 tumor bearing mice when the mean tumor volume was 100 mm^3. For all of the mice, transaxial T_1-weighted images were taken before injecting Gd-DTPA/m or Gd-DTPA as a control imaging. The mice were anesthetized with 1.8% isoflurane during the MRI experiments. The mice were injected i.v. with 0.22 mmol/kg of Gd-DTPA alone or 0.02 mmol/kg of Gd-DTPA/m based on Gd-DTPA. The transaxial T1W images were taken with a phantom containing water as a reference signal in defined time. The images were reconstructed and analyzed using ParaVision (Bruker Biospin) and Image J (NIH).

2.14. Element analysis using μ-SR-XRF

Micro-synchrotron radiation-induced X-ray fluorescence spectrometry imaging (μ-SR-XRF) was used to determine Gd-DTPA as well as Fe, Pt distribution in sections of solid tumor. Briefly, CDF_1 mice bearing C-26 tumor were intravenously injected with Gd-DTPA/m at 100 μg/mouse on a Gd-DTPA basis. Twenty-four hours later, tumors were collected and immediately frozen in acetone/dry ice, and then sliced using a cryostat and fixed on polypropylene sheets. μ-SR-XRF was performed using

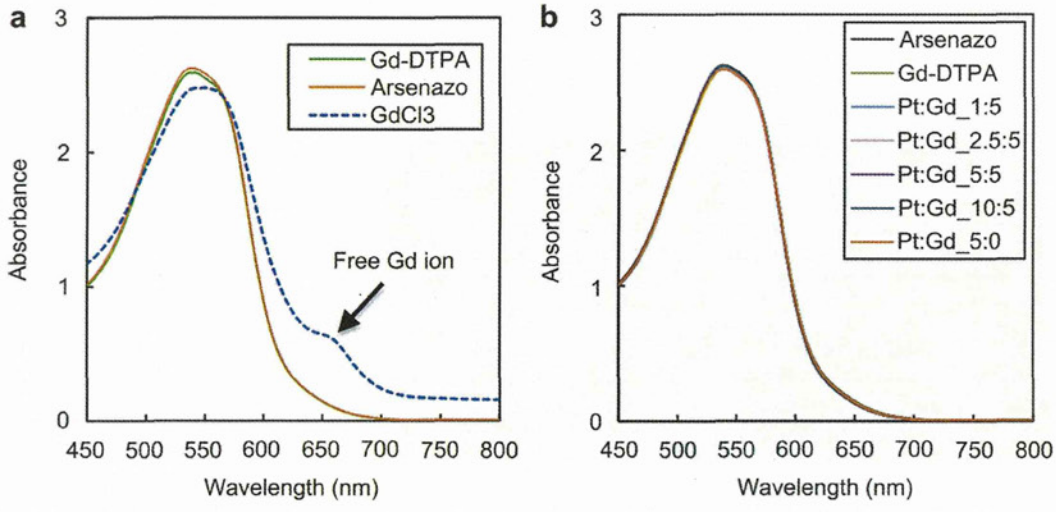

Fig. 2. Absorption spectrum of Arsenazo(III) solution with different mole ratios of Gd-DTPA and K_2PtCl_6 mixture solutions, the concentration of Gd-DTPA was maintained at 5 mM, the Pt concentration increased from 0 to 10 mM. The mixture of K_2PtCl_6 with Gd-DTPA did not compromise the stability of Gd-DTPA chelate.

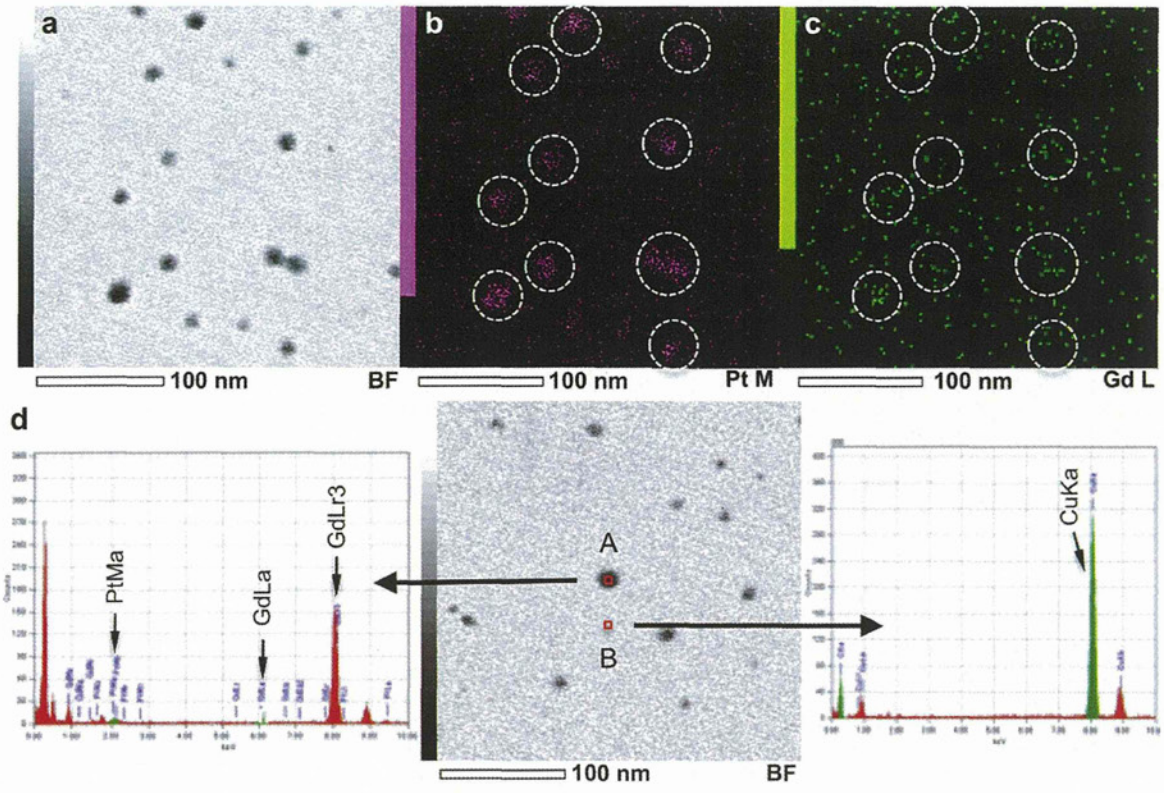

Fig. 3. EDS analysis of Gd-DTPA/m. (a) STEM image of Gd-DTPA/m. (b) Pt distribution under the STEM pattern. (c) Gd distribution under the STEM pattern. (d) EDX spectra of Gd-DTPA/m and background.

beam line 37XU at SPring-8 (Hyogo, Japan), operated at 8 GeV and ~100 mA. A photon beam with 14 keV of energy, a beam spot size of 1.3 × 1.3 μm^2, and an intensity of 1 × 10^{12} photons/s was used to irradiate the tissue sample. The fluorescence X-rays were measured using a Si-SSD in air at room temperature. Each sample on the acryl board was mounted on an *x*–*y* translation stage. The fluorescence X-ray intensity was normalized by the incident X-ray intensity, I_0, to produce a two-dimensional elemental map. An area of 250 × 250 μm^2 of the tissue sections was roughly scanned before μ-SR-XRF imaging.

3. Results and discussion

PEG-*b*-PAsp(DET) copolymers with different degree of polymerization (DP) (DP = 25, 35 and 45) were synthesized by aminolysis reaction of PEG-*b*-PBLA with diethylenetriamine (Scheme S1). PEG can hinder the interaction of the micelles with plasma proteins and prolong their circulation time in blood, while PAsp(DET) segments are minimally toxic and biodegradable as PAsp main-chain is fragmented from the nucleophilic attack of DET side chain via the formation of a succinimide ring [32]. Pt(IV) could form very stable chelates with amino groups of ethylenediamine and labile complexes with carboxylic groups [19,33]. Thus, as K_2PtCl_6 were mixed with PEG-*b*-PAsp(DET) and Gd-DTPA in aqueous solution, the block copolymers self-assembled into core–shell polymeric micelles carrying Gd-DTPA in the core as shown in Scheme 1. The K_2PtCl_6 concentration was found to be critical for the

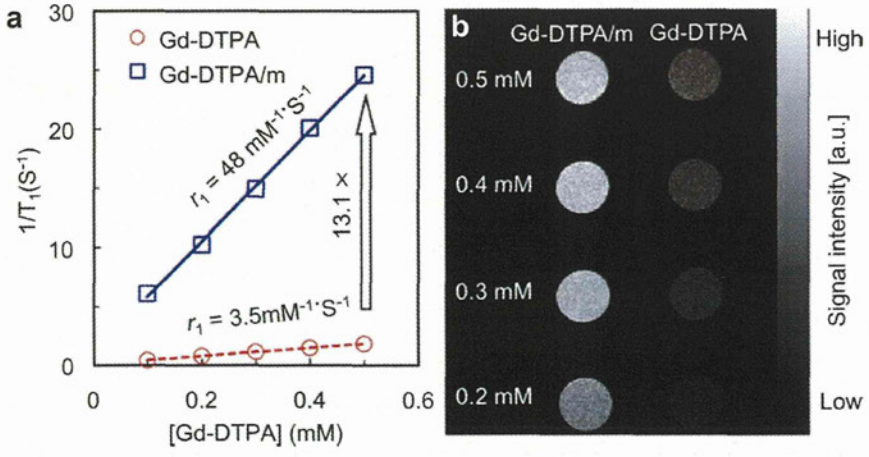

Fig. 4. MR enhancement effect of Gd-DTPA/m. (a) T_1 relaxivity coefficient. (b) T_1 weight MR images of Gd-DTPA/m and free Gd-DTPA solutions at 1 T.

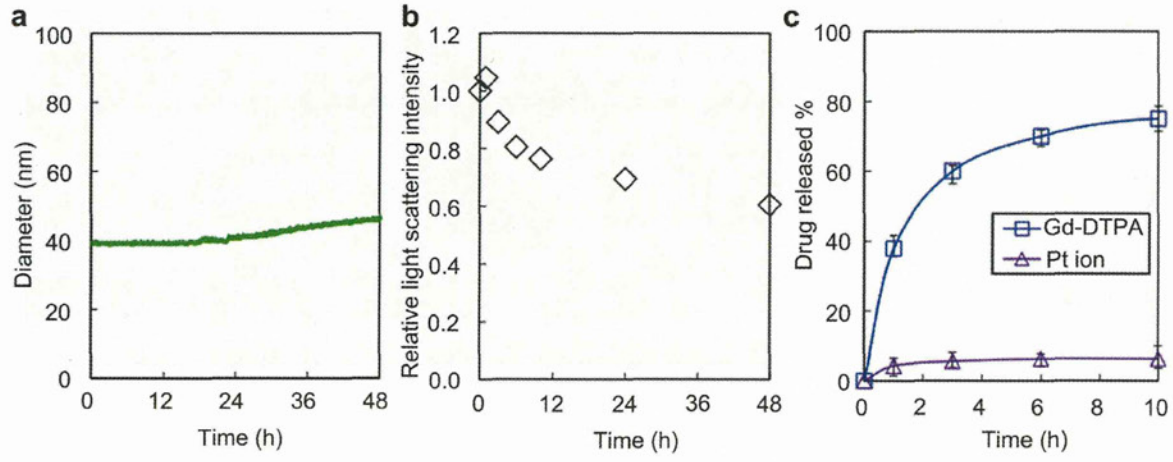

Fig. 5. Physicochemical characterization of Gd-DTPA/m under physiologic conditions. (a) Real time changes of diameter and (b) Change in relative light scattering intensity of Gd-DTPA/m. (c) Release rate of Gd-DTPA and Pt complexes from Gd-DTPA/m under similar conditions.

formation of micelles as without K_2PtCl_6, or even at low K_2PtCl_6 concentration, the micelles did not assemble (Fig. 1a and b). At 5 and 10 mM of K_2PtCl_6, narrowly distributed micelles were formed incorporating 16% and 12% of Gd-DTPA in weight, respectively (Table 1). Besides, the micelles prepared with PEG-*b*-Asp(DET) having longer PAsp(DET) segments showed higher loading of Gd-DTPA (DP = 45, 16%) than those PAsp(DET) with shorter segments (8% for DP = 25, and 9% for DP = 35) as shown in Table S1. Therefore, we decided to use Gd-DTPA/m prepared from PEG-*b*-PAsp(DET) (DP = 45), 5 mM Gd-DTPA and 5 mM K_2PtCl_6 for all of the following experiments as this composition produced micelles with highest Gd-DPTA loading. In addition, we confirmed that K_2PtCl_6 did not break the Gd-DTPA chelates as Gd^{3+} was not detectable, by arsenazo III method [31], at any ratio of Gd-DTPA/K_2PtCl_6 (Fig. 2).

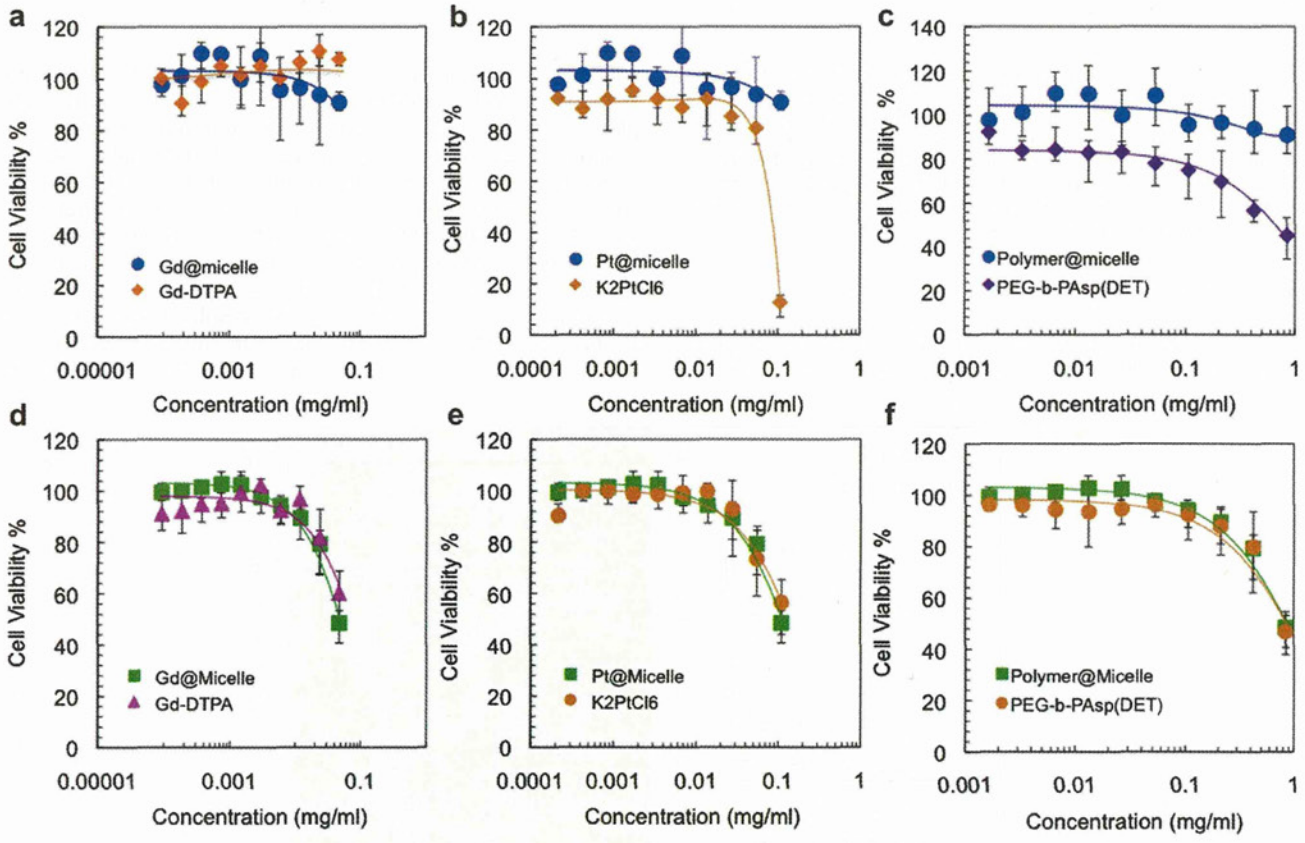

Fig. 6. Cytotoxicity of Gd-DTPA/m against HUVEC (a–c) and murine melanoma B16-F10 cells (d–f) after 72 h incubation. Micelles show comparable or even higher cell viability than free components, i.e., Gd-DTPA, K_2PtCl_6 and PEG-*b*-PAsp(DET).

The *z*-average diameter by intensity of these micelles was approximately 45 nm according to dynamic light scattering (Fig. 1c), and their zeta-potential was close to neutral at pH 7.4 (Figure S5). Diameter of sub-50 nm nanocarriers is important to achieve their deep tumor penetration in poorly permeable tumors according to our recent study [34]. Thus, the size of Gd-DTPA/m may be suitable for MR imaging of solid tumors with reduced permeability. According to TEM, Gd-DTPA/m showed quite narrowly distributed spherical morphology (Fig. 1d, e and Figure s6). Accordingly, the average size of the Gd-DTPA/m was calculated to be 22 nm (Fig. 1f), which is consistent with the number-averaged distribution (23 nm) calculated from *z*-averaged data obtained by DLS.

The elemental mapping under scanning TEM (STEM) and energy dispersive X-ray spectroscopy (EDS) of Gd-DTPA/m (Fig. 3) proved the existence of Gd and Pt elements inside the core of micelles. These results correlate with ICP-MS data (Table 1) as Pt concentration is higher than Gd encapsulated inside micelle.

The relaxivity of Gd-DTPA/m increased to 48 mM^{-1} s^{-1} based on Gd-DTPA, which is approximately 13-fold higher than that of free Gd-DTPA (Fig. 4a). T_1-weighted spin echo MRI at 1 T also revealed that Gd-DTPA/m highly improved MR contrast enhancement

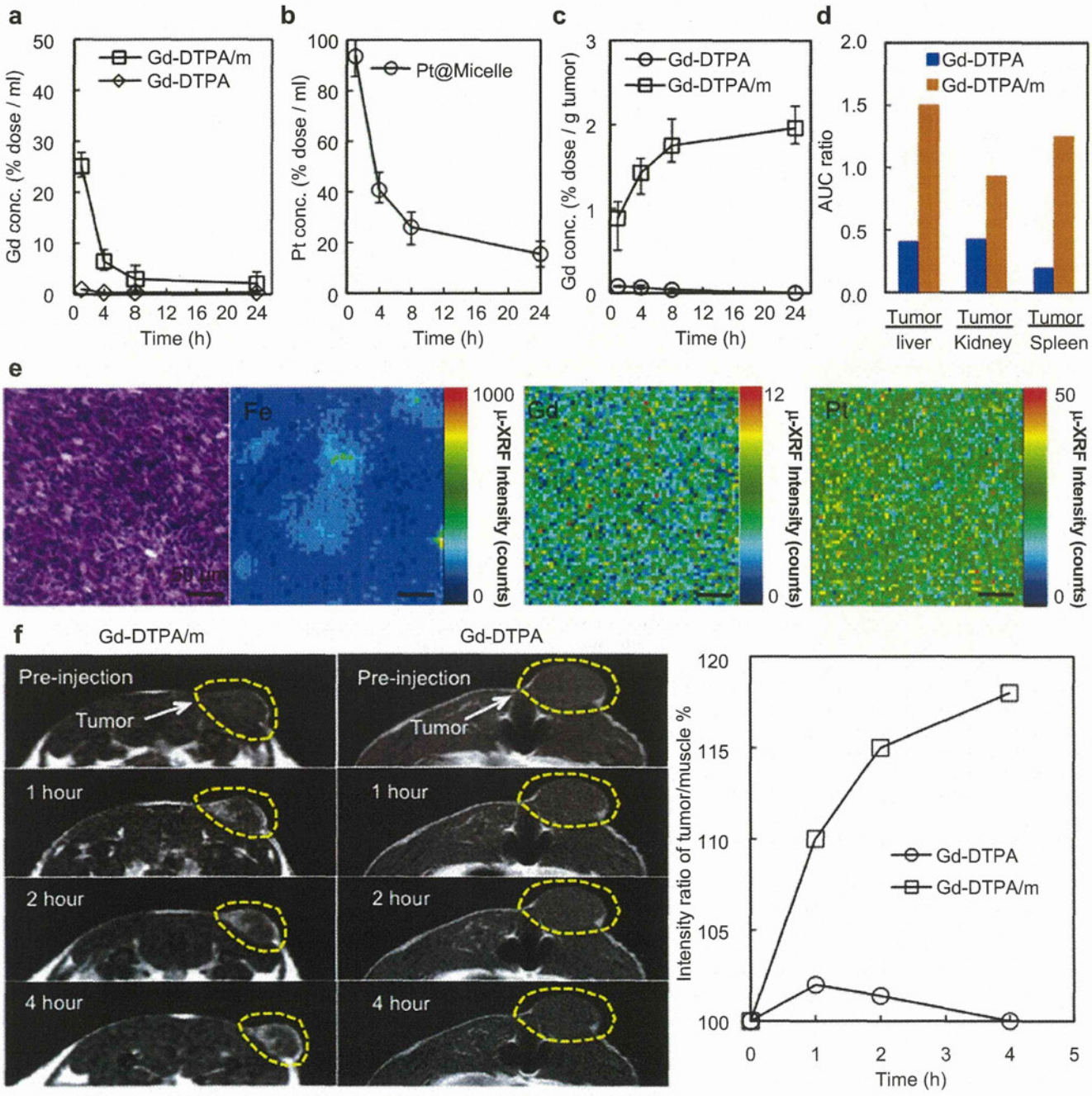

Fig. 7. *In vivo* evaluation of Gd-DTPA/m. (a) Plasma clearance of Gd-DTPA/m and free Gd-DTPA. (b) Plasma clearance of Pt@micelles. (c) Tumor accumulation of Gd-DTPA/m and free Gd-DTPA. (d) Tumor to tissue AUC ratios. (e) Microscopic findings (H&E staining) of tumor tissue and element distribution in tumor section. (f) T_1 weight tumor contrast enhancement after i.v. injection of Gd-DTPA loaded micelle and free Gd-DTPA.

compared to free Gd-DTPA (Fig. 3b), which may be attributed to a prolongation of the rotational correlation time, τ_R, due to restricted local motion similar to that of Gd-DTPA bound to macromolecules [35]. The benefits of slow rotation are observed at lower field strengths as the prevailing correlation time is almost always rotational diffusion, while at higher magnetic fields, the relaxivity of these Gd^{3+} complexes immobilized on slowly tumbling macromolecules rapidly decreases [36–38]. Accordingly, T_1-weighted spin echo MRI at 7 T showed that the contrast of Gd-DTPA/m was similar to free Gd-DTPA (Figure S7). Since clinical MRI machines use magnetic fields as high as 1.5 T, the design of Gd-DTPA/m is suitable for high relaxivity contrast enhancement at low dose. Interestingly, r_1 of Gd-DTPA/m augmented as the Pt/Gd ratio inside the core increased (Figure S8). Conversely, the r_1 relaxivity of Gd-DTPA/K_2PtCl_6 mixtures at different mole ratios or incubation time showed no significant r_1 relaxivity enhancement (Figure S9) suggesting that the incorporation of Gd-DTPA in the micelles core is necessary for the enhancement of relaxivity.

The micelles were stable under physiological conditions, i.e. in 10 mM PBS (pH 7.4) with 150 mM NaCl at 37 °C. In physiological environments, the diameter of the micelles slightly augmented after 18–20 h (Fig. 5a). Moreover, 60% of the initial light scattering intensity of the micelles was detectable even after 48 h (Fig. 5b). During the exposure of the micelles to physiological conditions, 75% Gd-DTPA was released in approximately 10 h, while only 7% of Pt was released probably due to stable metal complexation of Pt(IV) with PEG-*b*-PAsp(DET) (Fig. 5c). The ability of Gd-DTPA/m to sustainedly release Gd-DTPA, which can undergo glomerular filtration in the kidneys, may reduce the risk of free Gd discharge in the body.

Gd-DTPA/m was not cytotoxic against both primary cell lines (HUVEC) and tumor cell lines (B16-F10) (Fig. 6), suggesting its safety for *in vivo* application. Gd-DTPA/m extended the circulation of Gd-DTPA in the bloodstream, attaining 5% of the injected dose of Gd-DTPA after 8 h, while free Gd-DTPA was rapidly cleared from plasma (Fig. 7a and b). Moreover, approximately 15% of the injected Pt remained in the bloodstream after 24 h, which indicates the circulation of the micelles in the bloodstream. Gd-DTPA/m was able to deliver 26-fold higher CA in subcutaneous murine colon adenocarcinoma 26 (C-26) than free Gd-DTPA (Fig. 7c). In addition, the ratio of AUC in tumor versus organs indicated that Gd-DTPA/m improved the tumor-to-organ distribution of Gd-DTPA (Fig. 7d).

The microdistribution of the drugs at the tumor site was studied by micro-synchrotron radiation-induced X-ray fluorescence spectrometry imaging (μ-SR-XRF) of the tumor sites as Pt and Gd showed very distinct peaks in the sum spectrum of the line scan. Moreover, Fe mapping was also evaluated as it characterizes hemeproteins and therefore the positioning of blood vessels in the tissue. The atoms of Gd as well as Pt located in the whole tumor section in areas far from the Fe-rich regions suggesting deep tumor penetration and accumulation of Gd-DTPA/m as shown in Fig. 7e, in which the rainbow scales represent the quantity of element.

The size, neutral surface charge, stability and release characteristics of Gd-DTPA/m may contribute to the high penetration and accumulation of Gd-DTPA at the tumor site. The higher tumor accumulation and higher relaxivity of Gd-DTPA/m clearly and selectively enhanced the contrast at the tumor area in T_1-weighted MR images, even at low dose (0.02 mmol/kg based on Gd-DTPA) of contrast agents (Fig. 7f). The tumor selective contrast enhancement of Gd-DTPA/m was significant from 1 h after injection until the end of the experiment, that is, 4 h after injection. Oppositely, intravenously injected free Gd-DTPA, even at a 10 times higher dose, that is, 0.22 mmol/kg, failed to increase the intensity of the signal in the tumor region. These findings indicate the potential of GD-DTPA/m as a tumor-selective contrast agent.

4. Conclusion

Gd-DTPA/m efficiently improved the MRI-contrast of solid tumors demonstrating its potential application in the bio-imaging field. Accordingly, the sub-50 nm size, neutral surface and biological stability of Gd-DTPA/m, and the increased relaxivity of Gd-DTPA in the core of micelles lead to selective contrast enhancement of tumors. This facile and reversible metal complexation used for the construction of Gd-DTPA/m could also be applied for incorporating hydrophilic imaging probes, therapeutic drugs, or bioactive molecules into nanodevices for diagnosis and therapy. Accordingly, here, we illustrated a new approach for designing nano-sized vehicles by incorporating drugs via metal complexation besides widely used methods, such as covalent conjugation, or hydrophobic interaction, demonstrating its further application for loading compounds, which are difficult to incorporate in traditional nanocarriers.

Acknowledgments

This work was financially supported by the Japan Society for the Promotion of Science (JSPS) through its "Funding Program for World-Leading Innovative R&D on Science and Technology (FIRST Program)". TEM experiments were conducted in Research Hub for Advanced Nano Characterization, The University of Tokyo, supported by the Ministry of Education, Culture, Sports, Science and Technology (MEXT), Japan. P. M. acknowledges the fellowship from Ministry of Education, Science, Sports and Culture (MEXT), Japan. The authors are grateful Mr. Hashime Hoshi (JEOL), Ms. Sayaka Shibata and Aiko Sekita (NIRS) for technical support.

Appendix A. Supplementary data

Supplementary data related to this article can be found at http://dx.doi.org/10.1016/j.biomaterials.2012.09.030.

References

[1] Weissleder R, Pittet MJ. Imaging in the era of molecular oncology. Nature 2008;452:580–9.
[2] Mansfield P. Snapshot magnetic resonance imaging. Angew Chem Int Ed 2004; 43:5456–64.
[3] Weinmann HJ, Brasch RC, Press WR, Wesbey GE. Characteristics of gadolinium-DTPA complex: a potential NMR contrast agent. AJR Am J Roentgenol 1984; 142:619–24.
[4] Davis PL, Kaufman L, Crooks LE, Miller TR. Detectability of hepatomas in rat livers by nuclear magnetic resonance imaging. Invest Radiol 1981;16:354–9.
[5] Laurent S, Elst LV, Muller RN. Comparative study of the physicochemical properties of six clinical low molecular weight gadolinium contrast agents. Contrast Media Mol Imaging 2006;1:128–37.
[6] Ananta JS, Godin B, Sethi R, Moriggi L, Liu XW, Serda RE, et al. Geometrical confinement of gadolinium-based contrast agents in nanoporous particles enhances T-1 contrast. Nat Nanotech 2010;5:815–21.
[7] Thompson KH, Orvig C. Boon and bane of metal ions in medicine. Science 2003;300:936–9.
[8] Ferrari M. Cancer nanotechnology: opportunities and challenges. Nat Rev Cancer 2005;5:161–71.
[9] Cabral H, Nishiyama N, Kataoka K. Supramolecular nanodevices: from design validation to theranostic nanomedicine. Acc Chem Res 2011;44:999–1008.
[10] Kataoka K, Harada A, Nagasaki Y. Block copolymer micelles for drug delivery: design, characterization and biological significance. Adv Drug Deliv Rev 2001; 47:113–31.
[11] Nishiyama N, Morimoto Y, Jang WD, Kataoka K. Design and development of dendrimer photosensitizer-incorporated polymeric micelles for enhanced photodynamic therapy. Adv Drug Deliv Rev 2009;61:327–38.
[12] Rafi M, Cabral H, Kano MR, Mi P, Iwata C, Yashiro M, et al. Polymeric micelles incorporating (1,2-diaminocyclohexane)platinum (II) suppress the growth of orthotopic scirrhous gastric tumors and their lymph node metastasis. J Control Release 2012;159:189–96.
[13] Mikhaylov G, Mikac U, Magaeva AA, Itin VI, Naiden EP, Psakhye I, et al. Ferri-liposomes as an MRI-visible drug-delivery system for targeting tumours and their microenvironment. Nat Nanotech 2011;6:594–602.

[14] Floyd III WC, Klemm PJ, Smiles DE, Kohlgruber AC, Pierre VC, Mynar JL, et al. Conjugation effects of various linkers on Gd(III) MRI contrast agents with dendrimers: optimizing the hydroxypyridinonate (HOPO) ligands with nontoxic, degradable esteramide (EA) dendrimers for high relaxivity. J Am Chem Soc 2011;133:2390–3.
[15] Kojima C, Turkbey B, Ogawa M, Bernardo M, Regino CAS, Bryant LH, et al. Dendrimer-based MRI contrast agents: the effects of PEGylation on relaxivity and pharmacokinetics. Nanomedicine 2011;7:1001–8.
[16] Khemtong C, Kessinger CW, Ren J, Bey EA, Yang SG, Guthi JS, et al. In vivo off-resonance saturation magnetic resonance imaging of alphavbeta3-targeted superparamagnetic nanoparticles. Cancer Res 2009;69:1651–8.
[17] Mulder WJM, Strijkers GJ, van Tilborg GAF, Griffioen AW, Nicolay K. Lipid-based nanoparticles for contrast-enhanced MRI and molecular imaging. NMR Biomed 2006;19:142–64.
[18] Ai H. Layer-by-layer capsules for magnetic resonance imaging and drug delivery. Adv Drug Deliv Rev 2011;63:772–88.
[19] Vucic E, Sanders HM, Arena F, Terreno E, Aime S, Nicolay K, et al. Well-defined, multifunctional nanostructures of a paramagnetic lipid and a lipopeptide for macrophage imaging. J Am Chem Soc 2009;131:406–7.
[20] Kaida S, Cabral H, Kumagai M, Kishimura A, Terada Y, Sekino M, et al. Visible drug delivery by supramolecular nanocarriers directing to single-platformed diagnosis and therapy of pancreatic tumor model. Cancer Res 2010;70:7031–41.
[21] Nasongkla N, Bey E, Ren JM, Ai H, Khemtong C, Guthi JS, et al. Multifunctional polymeric micelles as cancer-targeted, MRI-ultrasensitive drug delivery systems. Nano Lett 2006;6:2427–30.
[22] Yokoyama M, Nakamura E, Makino K, Okano T, Yamamoto TA. Polymeric micelle MRI contrast agent with changeable relaxivity. J Control Release 2006; 114:325–33.
[23] Manus LM, Mastarone DJ, Waters EA, Zhang XQ, Schultz-Sikma EA, MacRenaris KW, et al. Gd(III)-nanodiamond conjugates for MRI contrast enhancement. Nano Lett 2010;10:484–9.
[24] Torchilin VP. PEG-based micelles as carriers of contrast agents for different imaging modalities. Adv Drug Deliv Rev 2002;54:235–52.
[25] Ai H, Flask C, Weinberg B, Shuai X, Pagel MD, Farrell D, et al. Magnetite-loaded polymeric micelles as ultrasensitive magnetic-resonance probes. Adv Mater 2005;17:1949–52.
[26] Duncan R, Izzo L. Dendrimer biocompatibility and toxicity. Adv Drug Deliv Rev 2005;57:2215–37.
[27] Matsumura Y, Kataoka K. Preclinical and clinical studies of anticancer agent-incorporating polymer micelles. Cancer Sci 2009;100:572–9.
[28] Plummer R, Wilson RH, Calvert H, Boddy AV, Griffin M, Sludden J, et al. A phase I clinical study of cisplatin-incorporated polymeric micelles (NC-6004) in patients with solid tumours. Br J Cancer 2011;104:593–8.
[29] Harada A, Kataoka K. Formation of polyion complex micelles in an aqueous milieu from a pair of oppositely-charged block-copolymers with poly(ethylene glycol) segments. Macromolecules 1995;28:5294–9.
[30] Kanayama N, Fukushima S, Nishiyama N, Itaka K, Jang WD, Miyata K, et al. A PEG-based biocompatible block catiomer with high buffering capacity for the construction of polyplex micelles showing efficient gene transfer toward primary cells. ChemMedChem 2006;1:439–44.
[31] Gouin S, Winnik FM. Quantitative assays of the amount of diethylene-triaminepentaacetic acid conjugated to water-soluble polymers using isothermal titration calorimetry and colorimetry. Bioconjug Chem 2001;12: 372–7.
[32] Itaka K, Ishii T, Hasegawa Y, Kataoka K. Biodegradable polyamino acid-based polycations as safe and effective gene carrier minimizing cumulative toxicity. Biomaterials 2010;31:3707–14.
[33] Iakovidis A, Hadjiliadis N. Complex-compounds of platinum(II) and platinum(IV) with amino-acids, peptides and their derivatives. Coord Chem Rev 1994;135:17–63.
[34] Cabral H, Matsumoto Y, Mizuno K, Chen Q, Murakami M, Kimura M, et al. Accumulation of sub-100nm polymeric micelles in poorly permeable tumours depends on size. Nat Nanotech 2011;6:815–23.
[35] Caravan P, Ellison JJ, McMurry TJ, Lauffer RB. Gadolinium(III) chelates as MRI contrast agents: structure, dynamics, and applications. Chem Rev 1999;99: 2293–352.
[36] Terreno E, Castelli DD, Viale A, Aime S. Challenges for molecular magnetic resonance imaging. Chem Rev 2010;110:3019–42.
[37] Mastarone DJ, Harrison VSR, Eckermann AL, Parigi G, Luchinat C, Meade TJ. A modular system for the synthesis of multiplexed magnetic resonance probes. J Am Chem Soc 2011;133:5329–37.
[38] Caravan P, Farrar CT, Frullano L, Uppal R. Influence of molecular parameters and increasing magnetic field strength on relaxivity of gadolinium- and manganese-based T1 contrast agents. Contrast Media Mol Imaging 2009;4: 89–100.

molecular pharmaceutics

Brief Article

pubs.acs.org/molecularpharmaceutics

Involvement of Ca^{2+} and ATP in Enhanced Gene Delivery by Bubble Liposomes and Ultrasound Exposure

Daiki Omata,[†] Yoichi Negishi,*[,†] Sho Yamamura,[†] Shoko Hagiwara,[†] Yoko Endo-Takahashi,[†] Ryo Suzuki,[‡] Kazuo Maruyama,[‡] Motoyoshi Nomizu,[§] and Yukihiko Aramaki[†]

[†]Department of Drug Delivery and Molecular Biopharmaceutics, School of Pharmacy, Tokyo University of Pharmacy and Life Sciences, Hachioji, Tokyo 192-0392, Japan

[‡]Department of Biopharmaceutics, School of Pharmaceutical Sciences, Teikyo University, Sagamihara, Kanagawa 252-5195, Japan

[§]Department of Clinical Biochemistry, School of Pharmacy, Tokyo University of Pharmacy and Life Sciences, Hachioji, Tokyo 192-0392, Japan

ABSTRACT: Recently, we reported the accelerated gene transfection efficiency of laminin-derived AG73-peptide-labeled polyethylene glycol-modified liposomes (AG73-PEG liposomes) and cell penetrating TAT-peptide labeled PEG liposomes using PEG-modified liposomes, which trap echo-contrast gas, "Bubble liposomes" (BLs), and ultrasound (US) exposure. BLs and US exposure were reported to enhance the endosomal escape of AG73-PEG liposomes, thereby leading to increased gene expression. However, the mechanism behind the effect of BLs and US exposure on endosomes is not well understood. US exposure was reported to induce an influx of calcium ions (Ca^{2+}) by enhancing permeability of the cell membrane. Therefore, we examined the effect of Ca^{2+} on the endosomal escape and transfection efficiency of AG73-PEG liposomes, which were previously enhanced by BLs and US exposure. For cells treated with EGTA, the endosomal escape and gene expression of AG73-PEG liposomes were not enhanced by BLs and US exposure. Similarly, transfection efficiency of the AG73-PEG liposomes in ATP-depleted cells was not enhanced. Our results suggest that Ca^{2+} and ATP are necessary for the enhanced endosomal escape and gene expression of AG73-PEG liposomes by BLs and US exposure. These findings may contribute to the development of useful techniques to improve endosomal escape and achieve efficient gene transfection.

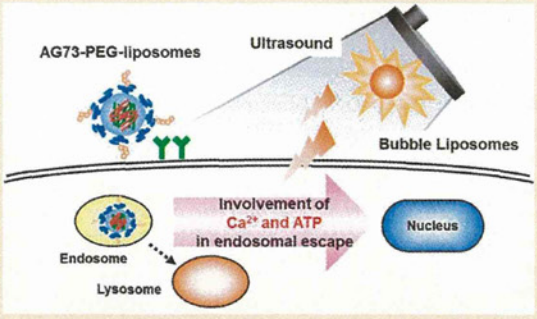

KEYWORDS: *AG73 peptide, atp, Bubble liposomes, calcium ions, gene delivery, endosomal escape, ultrasound*

INTRODUCTION

For successful gene therapy, various nonviral vectors such as lipid- and polymer-based carriers have been developed. However, they generally have relatively low transfection efficiencies, which need to be overcome.[1] Recent reports have emphasized the importance of subcellular and intracellular trafficking of gene delivery carriers. To achieve efficient gene transfection, carriers must overcome several steps including cellular internalization, endosomal escape, nuclear transfer and intracellular transcription.[2,3] Of these steps, endosomal escape is considered one of the most important, because most carriers are internalized into cells via an endocytic pathway. When escape from endosomes is impossible, the genes are degraded in lysosomes. Indeed, some groups have developed carriers and protocols that involve monitoring functions, such as pH sensitivity, temperature dependence, or photosensitivity, to deliver genes to the cytosol from endosomes.[4−7]

Previously, we developed laminin-derived AG73 peptide-labeled polyethylene glycol (PEG)-modified liposomes (AG73-PEG liposomes) as tumor targeted gene delivery carriers.[8] We also reported that the transfection efficiency of AG73-PEG liposomes and TAT-PEG liposomes, which were labeled with a TAT peptide (a cell penetrating peptide derived from human immunodeficiency virus trans-acting transcriptional activator), could be accelerated by PEG-modified liposomes, which trap echo-contrast gas, "Bubble liposomes" (BLs), and ultrasound (US) exposure.[9,10] BLs and US exposure enhanced the endosomal escape of AG73-PEG liposomes and TAT-PEG liposomes, leading to increased gene expression. However, the mechanism behind the effect of BLs and US exposure on endosomes and the resulting enhanced endosomal escape of carriers is not well understood. To promote this method as a more useful gene delivery tool, it is necessary to understand the detailed interactions at a fundamental level.

US pressure above a certain threshold can cause oscillating bubbles to undergo a violent collapse known as inertial cavitation. Microbubbles can be the nuclei of cavitation, and

Received: November 28, 2011
Revised: January 26, 2012
Accepted: March 2, 2012
Published: March 2, 2012

subsequent US exposure can induce more efficient cavitation. Inertial cavitation is thought to cause transient disruptions in cell membranes, which enable the transport of extracellular molecules into cells.[11−16] However, US exposure has also induced several biological effects, such as bone fracture healing, wound healing, and induction of apoptosis.[17−19] Moreover, the induced influx of calcium ions, the generation of reactive oxygen species, or the activation of some signals at a cellular level can be attributed to US exposure.[20−23]

Calcium ions (Ca^{2+}) have important roles in cells and are involved in various events such as cell proliferation and cell death.[24,25] US exposure induces the influx of Ca^{2+} by enhancing permeability of the cell membrane. Ca^{2+} also adjusts endosomal acidification and vesicle fusion.[26−29] Therefore, we focused on Ca^{2+} and hypothesized that BLs and US enhance the endosomal escape of gene delivery carriers via Ca^{2+} influx. We also investigated the involvement of ATP in enhanced gene delivery. In this study, we examined the effect of Ca^{2+} and ATP on the endosomal escape and transfection efficiency of AG73-PEG liposomes enhanced by BLs and US exposure.

EXPERIMENTAL SECTION

Materials. The pcDNA3-Luc plasmid, derived from pGL3-basic (Promega, Madison, WI), is an expression vector encoding the firefly luciferase gene under the control of a cytomegalovirus promoter. EGTA (ethylene glycol-bis(2-aminoethyl ether)-*N*,*N*,*N*′,*N*′-tetraacetic acid) was purchased from Sigma (St. Louis, MO). NaF and NaN_3 were purchased from Wako Pure Chemical Industries, Ltd. (Osaka, Japan). Antimycin A was purchased from Enzo Life Sciences, Inc. . (Farmingdale, NY). Alexa Fluor 488-conjugated transferrin was purchased from Molecular Probes, Inc. (Eugene, OR).

Cell Lines and Cultures. A 293T human embryonic kidney carcinoma cell line, stably overexpressing syndecan-2 (293T-Syn2 cell), was cultured in Dulbecco's modified Eagle's medium (DMEM; Kohjin Bio Co. Ltd., Tokyo, Japan), supplemented with 10% fetal bovine serum (FBS; Equitech Bio Inc., Kerrville, TX), penicillin (100 U/mL), streptomycin (100 μg/mL), and puromycin (0.4 μg/mL), at 37 °C in humidified 5% CO_2 atmosphere.

Preparation of AG73-PEG Liposomes. The Cys-AG73 peptide (CGG-RKRLQVQLSIRT) was synthesized manually using the 9-fluorenylmethoxycarbony (Fmoc)-based solid-phase strategy. The peptide was prepared in the COOH-terminal amide form and purified by reverse phase high-performance liquid chromatography. AG73-labeled PEG liposomes were prepared by the hydration method. The pDNA was diluted to a concentration of 0.1 mg/mL in 10 mM HEPES buffer (pH 7.4) and was condensed using 0.1 mg/mL poly-L-lysine (PLL); (SIGMA-Aldrich Co., St. Louis, MO). The complex of pDNA-PLL was added to a lipid film composed of 1,2-dioleoyl-*sn*-glycero-3-phospho-*rac*-1-glycerol (DOPG) (AVANTI Polar Lipids Inc., Alabaster, AL), 1,2-dioleoyl-*sn*-glycero-3-phosphoethanolamine (DOPE) (AVANTI Polar Lipids Inc., Alabaster, AL), and 1,2-distearoyl-*sn*-glycero-3-phosphatidylethanolamine-polyethylene glycol-maleimide (DSPE-PEG_{2000}-Mal) (NOF Corporation, Tokyo, Japan) in a molar ratio of 2:9:0.57 followed by incubation for 10 min at room temperature to hydrate the lipids. The solution was sonicated for 5 min in a bath-type sonicator (42 kHz, 100 W) (BRANSONIC 2510J-DTH, Bransoni Ultrasonic Co., Danbury, CT). For coupling, AG73 peptide, at a molar ratio of 5-fold DSPE-PEG_{2000}-Mal, was added to the PEG liposomes, and the mixture was incubated for 6 h at room temperature to conjugate the cysteine of Cys-AG73 peptide to the maleimide of the PEG liposomes using a thioether bond. The resulting AG73-peptide-conjugated PEG liposomes (AG73-PEG liposomes) were dialyzed to remove any excess peptide. AG73-PEG liposomes were modified with 5 mol % PEG and 3 mol % peptides.

Preparation of Bubble Liposomes. PEG liposomes composed of 1,2-dipalmitoyl-*sn*-glycero-3-phosphocholine (DPPC) (NOF Corporation, Tokyo, Japan) and 1,2-distearoyl-*sn*-glycero-3-phosphatidylethanolamine-polyethylene glycol (DSPE-PEG_{2000}-OMe) (NOF Corporation, Tokyo, Japan) in a molar ratio of 94:6 were prepared by a reverse-phase evaporation method. In brief, all reagents were dissolved in 1:1 (v/v) chloroform/diisopropyl ether. Phosphate buffered saline was added to the lipid solution, and the mixture was sonicated and then evaporated at 47 °C. The organic solvent was completely removed, and the size of the liposomes was adjusted to less than 200 nm using extruding equipment and a sizing filter (pore size: 200 nm) (Nuclepore Track-Etched Membrane, GE Healthcare, U.K.). The lipid concentration was measured using a Phospholipid C test Wako (Wako Pure Chemical Industries, Ltd., Osaka, Japan). BLs were prepared from liposomes using perfluoropropane gas (Takachio Chemical Ind. Co. Ltd., Tokyo, Japan). First, 2 mL sterilized vials containing 0.8 mL of the liposome suspension (lipid concentration: 1 mg/mL) were filled with perfluoropropane gas, capped, and then pressurized with a further 3 mL of perfluoropropane gas. The vials were placed in a bath-type sonicator (42 kHz, 100 W) (BRANSONIC 2510j-DTH, Branson Ultrasonics Co., Danbury, CT) for 5 min to form BLs.

Gene Transfection by AG73-PEG Liposomes with BLs and US Exposure. Two days before the experiments, 293T-Syn2 cells (1×10^5) were seeded in a 48-well plate. The cells were treated with AG73-PEG liposomes (encapsulating pDNA: 3 μg/mL) in serum-free medium for 4 h at 37 °C. The cells were washed twice with Ca^{2+}-free DMEM containing 10 mM EGTA. To deplete ATP, the cells were treated with NaN_3 (0.1%), NaF (10 mM), and antimycin A (1 μg/mL) for 30 min, and then the BLs were added. Within 2 min, US exposure was applied through a 6 mm diameter probe placed in the well (frequency, 2 MHz; duty, 50%; burst rate, 2 Hz; intensity, 1.0 W/cm^2; time, 10 s). A Sonopore 3000 (NEPA GENE, CO., Ltd., Chiba, Japan) was used to generate the US. The cells were transferred to fresh medium and cultured for 20 h, and then luciferase activity was determined.

Measurement of Luciferase Expression. Cell lysates were prepared with lysis buffer (0.1 M Tris-HCl pH 7.8, 0.1% Triton X-100, and 2 mM EDTA). Luciferase activity was measured as relative light units (RLU) per mg of protein using a luciferase assay system (Promega, Madison, WI) and a luminometer (LB96 V, Belthold Japan Co. Ltd., Tokyo, Japan).

Assessment of Localization of pDNA and Transferrin. The 293T-Syn2 cells (7×10^4) were seeded two days before the experiments. The cells were treated with AG73-PEG liposomes (Cy3-labeled pDNA: 3 μg/mL) and Alexa Fluor 488-conjugated transferrin (50 μg/mL) for 4 h at 37 °C. After incubation, the cells were washed, and the BLs (120 μg/mL) were added. Then, US exposure was applied (frequency, 2028 kHz; duty, 50%; burst rate, 2.0 Hz; intensity, 1.0 W/cm^2; time, 10 s). To assess the involvement of Ca^{2+} and ATP, the cells were treated as described in the above section. Subsequently, the cells were incubated for 10 min and then fixed with 4%

paraformaldehyde for 1 h at 4 °C followed by visualization using confocal laser scanning microscopy (CLSM). To differentiate the AG73-PEG liposomes internalized into the cytoplasm following attachment to the surface of the cell membrane, the cytoplasm was distinguished from the cell membrane as shown previously.[9,10,30,31] The rate of colocalization of Cy3-labeled pDNA with Alexa Fluor 488-conjugated transferrin was quantified as follows: amount of colocalization (%) = Cy3 $pixels_{colocalization}$/Cy3 $pixels_{total}$ × 100, where Cy3 $pixels_{colocalization}$ represents the number of Cy3 pixels colocalizing with Alexa Fluor 488-conjugated transferrin and Cy3 $pixels_{total}$ represents the total number of Cy3 pixels.

Assessment of Localization of pDNA and lamp-2. The 293T-Syn2 cells were first treated with AG73-PEG liposomes (Cy3-lableled pDNA: 3 μg/mL) for 4 h at 37 °C and then with BLs and US exposure. To assess the involvement of Ca^{2+} and ATP, cells were treated as described in the above section. Subsequently, the cells were incubated for 1 h and then fixed with 4% paraformaldehyde for 1 h at 4 °C. The cells were washed with PBS and permeabilized for 5 min in 0.2% saponin, followed by treatment with 10% goat serum in PBS. Finally, the cells were incubated with anti-lamp2 Ab (Santa Cruz Biotechnology, Inc., Santa Cruz, CA) overnight at 4 °C and treated with Alexa Fluor 488-conjugated secondary Ab (Invitrogen Co., Carlsbad, CA) for 1 h at room temperature in the dark. Then, CLSM and analysis was performed as described in the above section.

■ RESULTS AND DISCUSSION

In previous reports, we have showed that BLs and US exposure could enhance endosomal escape and gene transfection of AG73-PEG liposomes. We have proposed the mechanism that the cavitation induced in the outside of cells by US exposure and BLs could affect endosomes, and then AG73-PEG liposomes internalized by endocytosis escaped from endosomes, leading to enhanced gene expression. It have been also confirmed that AG73-PEG liposomes could not be introduced into cytoplasm directly through the cell membrane after the US-mediated disruption of BLs. However, the exact mechanism of accelerated endosomal escape of carriers was not clear. US exposure induces the influx of Ca^{2+} by enhancing permeability of the cell membrane.[21] In addition, Ca^{2+} adjusts endosomal acidification and vesicle fusion.[26−29] Therefore, to evaluate the mechanism by which BLs and US exposure could promote the endosomal escape of AG73-PEG liposomes, we examined the effect of Ca^{2+} on the endosomal escape and transfection efficiency of AG73-PEG liposomes enhanced by BLs and US exposure. ATP is involved in various reactions, such as acidification of endosomes, intracellular trafficking of vesicles and fusion of vesicles.[26] We also investigated the involvement of ATP-dependent processes in enhanced gene delivery.

First, to evaluate the involvement of Ca^{2+} and ATP in gene expression enhanced by BLs and US exposure, we examined the effect of Ca^{2+} and ATP on gene expression efficiency of AG73-PEG liposomes using 293T-Syn2 cells. The cells were incubated with AG73-PEG liposomes containing pcDNA3-Luc, and then treated with BLs and US exposure. After 20 h incubation, luciferase activity was assayed. BLs and US exposure enhanced the luciferase activity of AG73-PEG liposomes by approximately 60-fold compared to that of AG73-PEG liposomes alone.[9] By contrast, when the cells were treated with 10 mM EGTA before the treatment of BLs and US exposure, the enhancement ratio of luciferase activity by BLs and US exposure was decreased. To examine the effect of ATP on gene transfection efficiency, the cells were treated with NaN_3, NaF, and antimycin A to deplete ATP. The subsequent luciferase assay showed insignificant enhancement by BLs and US exposure. Conversely, when cells were treated with AG73-PEG liposomes alone, luciferase activity was not affected by Ca^{2+} and ATP depletion (Figure 1). These results suggest that

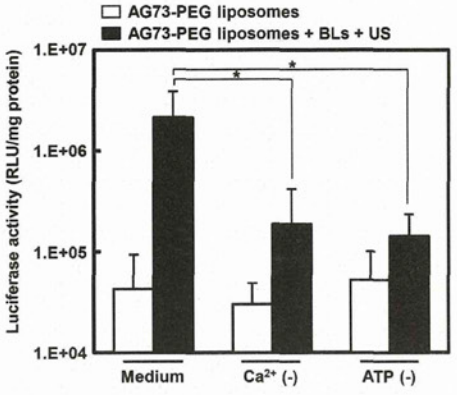

Figure 1. Effects of Ca^{2+} and ATP on gene expression by AG73-PEG liposomes with BLs and US exposure. 293T-Syn2 cells were treated with AG73-PEG liposomes for 4 h at 37 °C, and then cells were washed twice with Ca^{2+}-free DMEM containing 10 mM EGTA for a depleted Ca^{2+} condition. ATP was depleted by pretreating cells for 30 min before US exposure with 1 μg/mL antimycin A, 10 mM NaF, and 0.1% NaN_3. BLs (120 μg/mL) were added to cells followed by immediate US exposure. After replacement with fresh medium, the cells were cultured for 20 h and luciferase activity was determined. The data are shown as the means ± SD (n = 4). *p < 0.05.

Ca^{2+} and ATP may be necessary to enhance gene transfection efficiency of AG73-PEG liposomes by BLs and US exposure. On the other hand, it is reported that extracellular Ca^{2+} plays important roles to repair the cell membrane disruption and maintain cell survival.[32] Therefore, we examined the cell viability in Ca^{2+}-depleted condition. As a result, in this condition, the cell viability had almost no difference in the treatment with or without BLs and US exposure (data not shown). This result suggested that the decreased enhancement ratio of luciferase activity by the treatment of BLs and US exposure in Ca^{2+}-depleted condition was not due to a change of cell viability.

Recent reports have emphasized the importance of subcellular and intracellular trafficking of gene delivery carriers.[2,3] Among the several steps involeved, endosomal escape is considered one of the most important. In previous study, we have reported that enhanced endosomal escape of AG73-PEG liposomes by BLs and US exposure could increase gene expression.[9] Therefore, we evaluated the involvement of Ca^{2+} and ATP on the endosomal escape of gene delivery carriers. We examined the effects of Ca^{2+} and ATP on localization of pDNA encapsulated in AG73-PEG liposomes and transferrin, as an endosome marker,[33] by confocal microscopy. BLs and US exposure enhanced the endosomal escape of AG73-PEG liposomes and decreased the ratio of colocalization of pDNA and transferrin.[9] The 293T-Syn2 cells were first incubated with AG73-PEG liposomes containing Cy3-labeled pDNA and Alexa Fluor 488-conjugated transferrin and then treated with BLs and US exposure. The cells were observed by confocal microscopy to assess the colocalization of

Cy3-labeled pDNA and Alexa Fluor 488-conjugated transferrin. As shown in Figure 2a, the pDNA internalized into cells were

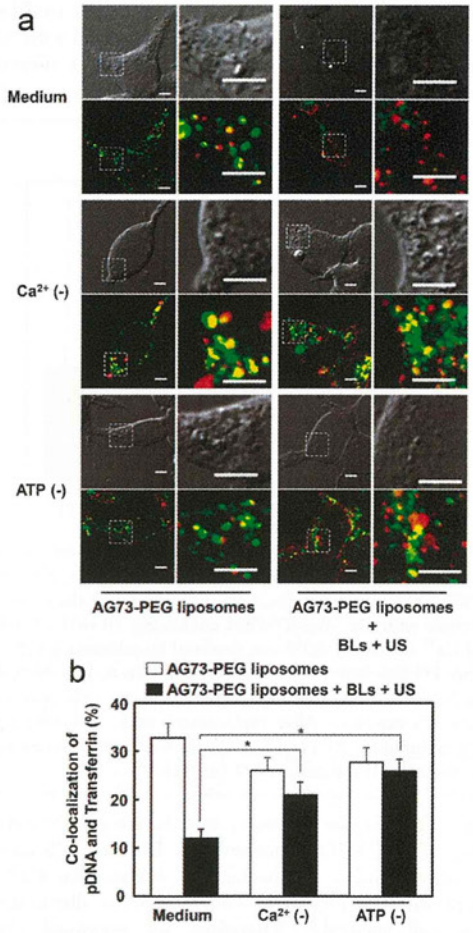

Figure 2. Effects of Ca^{2+} and ATP on intracellular localization of pDNA and endosomes. (a, b) The 293T-Syn2 cells were treated with AG73-PEG liposomes encapsulating Cy3-labeled pDNA (red) and Alexa Fluor 488-conjugated transferrin (green) for 4 h at 37 °C and then washed twice with Ca^{2+}-free DMEM containing 10 mM EGTA to create Ca^{2+}-depleted conditions. ATP was depleted by pretreating cells for 30 min before US exposure with 1 μg/mL antimycin A, 10 mM NaF, and 0.1% NaN_3. BLs (120 μg/mL) were added to cells followed by immediate US exposure. The cells were incubated for 10 min, fixed with 4% paraformaldehyde for 1 h at 4 °C and observed by CLSM. The areas within the dotted square are shown as enlarged images. The scale bars represent 5 μm. The ratio of colocalization of Cy3-labeled pDNA with Alexa Fluor 488-conjugated transferrin was quantified. The data are shown as means ± SE (n = 50). *p < 0.05 compared with AG73-PEG liposomes alone (Mann–Whitney's U test).

colocalized with transferrin, whereas BLs and US exposure decreased the colocalization of the pDNA and transferrin. However, when cells were treated with 10 mM EGTA, BLs and US exposure did not affect the intracellular localization of the pDNA and transferrin. In the ATP-depleted state, BLs and US exposure had no effect on the intracellular localization of the pDNA and transferrin. Furthermore, we calculated the ratio of colocalization of the pDNA and transferrin and found that BLs and US exposure decreased the ratio of colocalization. By contrast, when cells were treated with 10 mM EGTA or were exposed in an ATP-depleted state, BLs and US exposure did not affect the ratio of colocalization of pDNA and transferrin (Figure 2b). These results suggest that Ca^{2+} and ATP may be required for endosomal escape of AG73-PEG liposomes after the addition of BLs and US exposure.

Efficient gene transfection requires sufficient delivery of genes from the endosomes to the cytosol, to avoid the degradation of genes in lysosomes. Therefore, we assessed the intracellular localization of pDNA and lysosomes and the effects of Ca^{2+} and ATP on localization of pDNA and lysosomes. The 293T-Syn2 cells were treated with AG73-PEG liposomes containing Cy3-labeled pDNA, followed by the addition of BLs and application of US. The cells were fixed and stained with antibodies for lamp-2, a lysosome marker.[34] As a result, the pDNA internalized into cells was colocalized with lamp-2 at 10 or 60 min, whereas BLs and US exposure decreased the colocalization of pDNA and lamp-2 at 60 min after US exposure (Figure3). Moreover, when cells were treated with 10 mM EGTA and depleted of ATP, BLs and US exposure did not decrease the localization of pDNA and lamp-2 (Figure

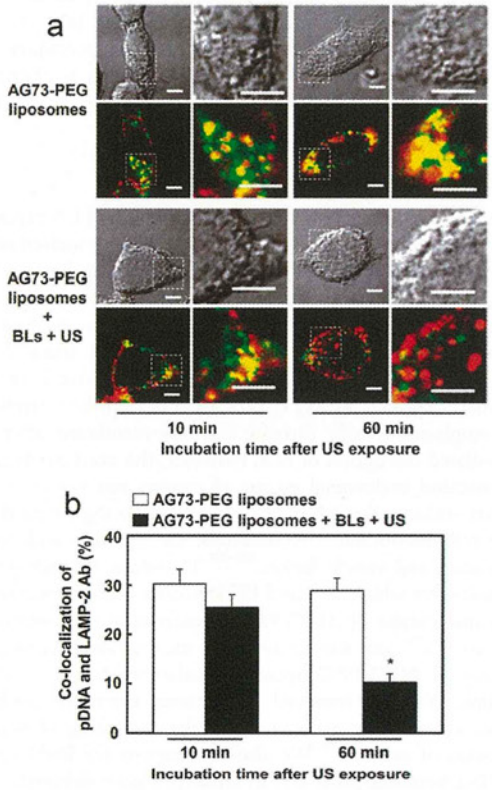

Figure 3. Effect of BLs and US exposure on intracellular localization of pDNA and lysosomes. The 293T-Syn2 cells were treated with AG73-PEG liposomes encapsulating Cy3-labeled pDNA (red) for 4 h at 37 °C. BLs (120 μg/mL) were added to cells followed by immediate US exposure. The cells were incubated for 10 or 60 min and then fixed with 4% paraformaldehyde for 1 h at 4 °C followed by staining with antibodies for lamp-2 (green), a marker for lysosomes. The cells were observed by CLSM. The areas within the dotted square are shown as enlarged images. The scale bars represent 5 μm. The ratio of colocalization of Cy3-labeled pDNA with lamp-2 was quantified. The data are shown as means ± SE (n = 50). *p < 0.05 (Mann–Whitney's U test).

dx.doi.org/10.1021/mp200606d | Mol. Pharmaceutics 2012, 9, 1017–1023

4a). We also evaluated the ratio of colocalization of pDNA and lamp-2. In normal medium, the ratio of colocalization of pDNA and lamp-2 was decreased by the application of BLs and US. By contrast, the decrease in the ratio of colocalization of pDNA and lamp-2 could be abrogated by 10 mM EGTA and ATP depletion (Figure 4b). These results suggest that BLs and US exposure could decrease the ratio of colocalization of pDNA and lysosomes. Furthermore, Ca^{2+} and ATP may be involved in the escape of AG73-PEG liposomes from lysosomes. We also confirmed the change of localization of pDNA with endosomes or lysosomes. When 293T-Syn2 cells were treated by AG73-PEG liposomes with BLs and US exposure, a decrease in colocalization of pDNA and endosomes was observed at 10 min after US exposure,[9] whereas a decrease in colocalization of pDNA and lysosomes was observed at 60 min after US exposure (Figure 3). These results suggest that BLs and US exposure might significantly affect endosomes, leading to the decrease in colocalization of pDNA and endosomes. In addition, the increase in the release of genes to the cytosol from endosomes might decrease gene delivery from endosomes to lysosomes.

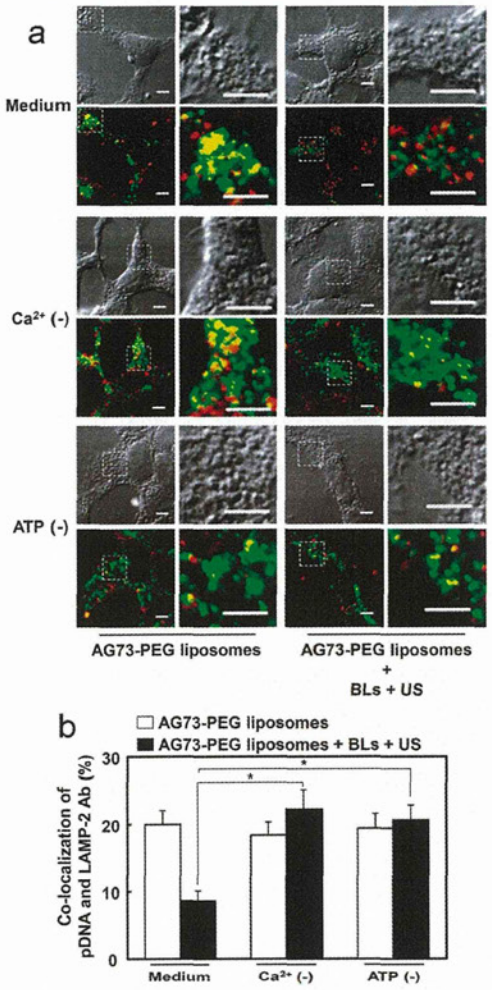

Figure 4. Effects of Ca^{2+} and ATP on intracellular localization of pDNA and lysosome. (a, b) The 293T-Syn2 cells were treated with AG73-PEG liposomes encapsulating Cy3-labeled pDNA (red) for 4 h at 37 °C and then washed twice with Ca^{2+}-free DMEM containing 10 mM EGTA to create Ca^{2+}-depleted conditions. ATP was depleted by pretreating cells for 30 min before US exposure with 1 μg/mL antimycin A, 10 mM NaF, and 0.1% NaN_3. BLs (120 μg/mL) were added to cells followed by immediate US exposure. The cells were incubated for 1 h, fixed with 4% paraformaldehyde for 1 h at 4 °C and stained with antibodies for lamp-2 (green), a marker for lysosomes. The cells were observed by CLSM. The areas within the dotted square are shown as enlarged images. The scale bars represent 5 μm. The ratio of colocalization of Cy3-labeled pDNA with lamp-2 was quantified. The data are shown as means ± SE (n = 50). *p < 0.05 (Mann–Whitney's U test).

Although Ca^{2+} and ATP were involved in enhanced endosomal escape and gene expression efficiency of AG73-PEG liposomes by BLs and US exposure, how Ca^{2+} and ATP enhance the endosomal escape of carriers is still unclear. More investigations into the detailed mechanism of enhanced endosomal escape of AG73-PEG liposomes by BLs and US exposure are required. Moreover, endosomal acidification is adjusted by Ca^{2+}, suggesting that the influx of Ca^{2+} by BL and US exposure may affect endosomal acidification.[26] This could lead to the destabilization of endosomes and hydrogen pumps, such as H^+/K^+-ATPase. However, Ca^{2+} and ATP are involved in endosomal membrane fusion.[27,28] Therefore, an influx of Ca^{2+} by BLs and US exposure and ATP may affect endosomal membrane fusion. Our study demonstrated the involvement of Ca^{2+} and ATP in enhanced endosomal escape and gene expression efficiency of AG73-PEG liposomes by BLs and US exposure. Significantly, BLs and US exposure enhanced endosomal escape through biological effects rather than physical effects. In fact, our results suggest that BLs and US exposure could affect more endosomes than lysosomes. It is expected that BLs and US exposure could be safer tools for the enhancement of endosomal escape by setting the appropriate US exposure conditions.

In conclusion, our study focused on Ca^{2+} and ATP and investigated the particular mechanism of enhanced endosomal escape and gene expression of AG73-PEG liposomes by BLs and US exposure. When cells were treated in Ca^{2+}- and ATP-depleted conditions, endosomal escape and gene expression of AG73-PEG liposomes were not enhanced by BLs and US exposure. These results suggest that both Ca^{2+} and ATP are necessary for enhanced endosomal escape and gene expression of AG73-PEG liposomes by BLs and US exposure. These findings may contribute to the development of useful gene transfection methods to achieve efficient gene transfection by improving endosomal escape.

■ AUTHOR INFORMATION

Corresponding Author

*Tokyo University of Pharmacy and Life Sciences, School of Pharmacy, Drug and Gene Delivery Systems, 1432-1

Horinouchi, Hachioji, Tokyo 192-0392, Japan. Tel and fax: +81-42-676-3183. E-mail: negishi@toyaku.ac.jp.

Notes

The authors declare no competing financial interest.

■ ACKNOWLEDGMENTS

We are grateful to Dr. Katsuro Tachibana (Department of Anatomy, School of Medicine, Fukuoka University) for technical advice regarding the induction of cavitation with US, and to Yasuhiko Hayakawa and Kosho Suzuki (NEPAGENE Co., LTD.) for technical advice regarding exposure to US. This study was supported by an Industrial Technology Research Grant (04A05010) from the New Energy and Industrial Technology Development Organization (NEDO) of Japan, a Grant-in-aid for Exploratory Research (18650146) and a Grant-in-aid for Scientific Research (B) (20300179) from the Japan Society for the Promotion of Science, and by a grant for private universities provided by the Promotion and Mutual Aid Corporation for Private Schools of Japan.

■ ABBREVIATIONS USED

BLs, Bubble liposomes; CLSM, confocal laser scanning microscopy; DOPE, 1,2-dioleoyl-*sn*-glycero-3-phosphoethanolamine; DOPG, 1,2-dioleoyl-*sn*-glycero-3-phospho-*rac*-1-glycerol; DSPE, 1,2-distearoyl-*sn*-glycero-3-phosphatidylethanolamine; FBS, fetal bovine serum; Fmoc, fluorenylmethoxycarbonyl; Mal, maleimide; pDNA, plasmid DNA; PEG, polyethylene glycol; US, ultrasound

■ REFERENCES

(1) Zhang, S.; Xu, Y.; Wang, B.; Qiao, W.; Liu, D.; Li, Z. Cationic compounds used in lipoplexes and polyplexes for gene delivery. *J. Controlled Release* **2004**, *100*, 165−180.

(2) Hama, S.; Akita, H.; Ito, R.; Mizuguchi, H.; Hayakawa, T.; Harashima, H. Quantitative comparison of intracellular trafficking and nuclear transcription between adenoviral and lipoplex systems. *Mol. Ther.* **2006**, *13*, 786−794.

(3) Varga, C. M.; Tedford, N. C.; Thomas, M.; Klibanov, A. M.; Griffith, L. G.; Auffenburger, D. A. Quantitative comparison of polyethylenimine formulations and adenoviral vectors in terms of intracellular gene delivery processes. *Gene Ther.* **2005**, *12*, 1023−1032.

(4) Hatakeyama, H.; Ito, E.; Akita, H.; Oishi, M.; Nagasaki, Y.; Futaki, S.; Harashima, H. A pH-sensitive fusogenic peptide facilitates endosomal escape and greatly enhances the gene silencing of siRNA-containing nanoparticles in vitro and in vivo. *J. Controlled Release* **2009**, *139*, 127−132.

(5) Subbarao, N. K.; Parente, R. A.; Szoka, F. C.; Nadasdi, L.; Pongracz, K. pH-dependent bilayer destabilization by an amphipathic peptide. *Biochemistry* **1987**, *26*, 2964−2972.

(6) Lee, S. H.; Choi, S. H.; Kim, S. H.; Park, T. G. Thermally sensitive cationic polymer nanocapsules for specific cytosolic delivery and efficient gene silencing of siRNA: swelling induced physical disruption of endosome by cold shock. *J. Controlled Release* **2008**, *125*, 25−32.

(7) Høgset, A.; Prasmickaite, L.; Selbo, P. K.; Hellum, M.; Engesaeter, B. Ø.; Bonsted, A.; Berg, K. Photochemical internalisation in drug and gene delivery. *Adv. Drug Delivery Rev.* **2004**, *56*, 95−115.

(8) Negishi, Y.; Omata, D.; Iijima, H.; Hamano, N.; Endo-Takahashi, Y.; Nomizu, M.; Aramaki, Y. Preparation and characterization of laminin-derived peptide AG73-coated liposomes as a selective gene delivery tool. *Biol. Pharm. Bull.* **2010**, *33*, 1766−1769.

(9) Negishi, Y.; Omata, D.; Iijima, H.; Takabayashi, Y.; Suzuki, K.; Endo, Y.; Suzuki, R.; Maruyama, K.; Nomizu, M.; Aramaki, Y. Enhanced laminin-derived peptide AG73-mediated liposomal gene transfer by bubble liposomes and ultrasound. *Mol. Pharmaceutics* **2010**, *7*, 217−226.

(10) Omata, D.; Negishi, Y.; Hagiwara, S.; Yamamura, S.; Endo-Takahashi, Y.; Suzuki, R.; Maruyama, K.; Nomizu, M.; Aramaki, Y. Bubble liposomes and ultrasound promoted endosomal escape of TAT-PEG liposomes as gene delivery carriers. *Mol. Pharmaceutics* **2011**, *8* (6), 2416−2423.

(11) Delius, M.; Adams, G. Shock wave permeabilization with ribosome inactivating proteins; a new approach to tumor therapy. *Cancer Res.* **1999**, *59*, 5227−5232.

(12) Taniyam, Y.; Tachibana, K.; Hiraoka, K.; Aoki, M.; Yamamoto, S.; Matsumoto, K.; Nakamura, T.; Ogihara, T.; Kaneda, Y.; Morishita, R. Development of safe and efficient novel nonviral gene transfer using ultrasound: enhancement of transfection efficiency of naked plasmid DNA in skeletal muscle. *Gene Ther.* **2002**, *9*, 260−269.

(13) Negishi, Y.; Matsuo, K.; Endo-Takahashi, Y.; Suzuki, K.; Matsuki, Y.; Takagi, N.; Suzuki, R.; Maruyama, K.; Aramaki, Y. Delivery of an angiogenic gene into ischemic muscle by novel bubble liposomes followed by ultrasound exposure. *Pharm. Res.* **2011**, *28*, 712−719.

(14) Negishi, Y.; Endo, Y.; Fukuyama, T.; Suzuki, R.; Takizawa, T.; Omata, D.; Maruyama, K.; Aramaki, Y. Delivery of siRNA into the cytoplasm by liposomal bubbles and ultrasound. *J. Controlled Release* **2008**, *132*, 124−130.

(15) Negishi, Y.; Endo-Takahashi, Y.; Ishii, K.; Suzuki, R.; Oguri, Y.; Murakami, T.; Maruyama, K.; Aramaki, Y. Development of novel nucleic acid-loaded bubble liposomes using cholesterol-conjugated siRNA. *J. Drug Targeting* **2011**, *19*, 830−836.

(16) Suzuki, R.; Namai, E.; Oda, Y.; Nishiie, N.; Otake, S.; Koshima, R.; Hirata, K.; Taira, Y.; Utoguchi, N.; Negishi, Y.; Nakagawa, S.; Maruyama, K. Cancer gene therapy by IL-12 gene delivery using liposomal bubbles and tumoral ultrasound exposure. *J. Controlled Release* **2010**, *142*, 245−250.

(17) Warden, S. J.; Fuchs, R. K.; Kessler, C. K.; Avin, K. G.; Cardinal, R. E.; Stewart, R. L. Ultrasound produced by a conventional therapeutic ultrasound unit accelerates fracture repair. *Phys. Ther.* **2006**, *86*, 1118−1127.

(18) Warden, S. J. A new direction for ultrasound therapy in sports medicine. *Sports Med.* **2003**, *33*, 95−107.

(19) Feril, L. B. Jr.; Kondo, T.; Zhac, Q. L.; Ogawa, R.; Tachibana, K.; Kudo, N.; Fujimoto, S.; Nakamura, S. Enhancement of ultrasound-induced apoptosis and cell lysis by echo-contrast agents. *Ultrasound Med. Biol.* **2003**, *29*, 331−337.

(20) Juffermans, L. J.; Dijkmans, P. A.; Musters, R. J.; Visser, C. A.; Kamp, O. Transient permeabilization of cell membranes by ultrasound-exposed microbubbles is related to formation of hydrogen peroxide. *Am. J. Physiol.* **2006**, *291*, H1595−H1601.

(21) Juffermans, L. J.; Kamp, O.; Dijkmans, P. A.; Visser, C. A.; Musters, R. J. Low-intensity ultrasound-exposed microbubbles provoke local hyperpolarization of the cell membrane via activation of BK(Ca) channels. *Ultrasound Med. Biol.* **2008**, *34*, 502−508.

(22) Zhou, Y.; Shi, J.; Cui, J.; Deng, C. X. Effects of extracellular calcium on cell membrane resealing in sonoporation. *J. Controlled Release* **2008**, *126*, 34−43.

(23) Takeuchi, R.; Ryo, A.; Komitsu, N.; Mikuni-Takagaki, Y.; Fukui, A.; Takagi, Y.; Shiraishi, T.; Morishita, S.; Yamazaki, Y.; Kumagai, K.; Aoki, I.; Saito, T. Low-intensity pulsed ultrasound activates the phosphatidylinositol 3 kinase/AKT pathway and stimulates the growth of chondrocytes in three-dimensional cultures: a basic science study. *Arthritis Res. Ther.* **2008**, *10*, R77.

(24) Giacomello, M.; Drago, I.; Pizzo, P.; Pozzan, T. Mitochondrial Ca^{2+} as a key regurator of cell life and death. *Cell Death Differ.* **2007**, *14*, 1267−1274.

(25) Hassan, M. A.; Cambell, P.; Kondo, T. The role of Ca^{2+} in ultrasound-elicited bioeffects: progress, perspective and prospects. *Drug Discovery Today* **2010**, *15*, 892−906.

(26) Lelouvier, B.; Puertollano, R. Mucolipin-3 regulates luminal calcium, acidification, and membrane fusion in the endosomal pathway. *J. Biol. Chem.* **2011**, *286*, 9826−9832.

(27) Yan, Q.; Sun, W.; McNew, J. A.; Vida, T. A.; Bean, A. J. Ca^{2+} and N-ethylmaleimide-sensitive factor differentially regulate disassembly of SNARE complexes on early endosomes. *J. Biol. Chem.* **2004**, *279*, 18270−18276.
(28) Mayorga, L. S.; Berón, W.; Sarrouf, M. N.; Colombo, M. I.; Creutz, C.; Stahl, P. D. Calcium-dependent fusion among endosomes. *J. Biol. Chem.* **1994**, *269*, 30927−30934.
(29) Rescher, U.; Zobiack, N.; Gerke, V. Intact Ca2+-binding sites are required for targeting of annxin 1 to endosomal membranes in living HeLa cells. *J. Cell Sci.* **2000**, *113*, 3931−3938.
(30) Suh, J.; Wirtz, D.; Hanes, J. Efficient active transport of gene nanocarriers to the cell nucleus. *Proc. Natl. Acad. Sci. U.S.A.* **2003**, *100*, 3878−3882.
(31) Oba, M.; Aoyagi, K.; Miyata, K.; Matsumoto, Y.; Itaka, K.; Nishiyama, N.; Yamasaki, Y.; Koyama, H.; Kataoka, K. Polyplex micelles with cyclic RGD peptide ligands and disulfide cross-links directing to the enhanced transfection via controlled intracellular trafficking. *Mol. Pharmaceutics* **2008**, *5*, 1080−1092.
(32) Idone, V.; Tam, C.; Goss, J. W.; Toomre, D.; Pypaert, M.; Andrews, N. W. Repair of injured plasma membrane by rapid Ca^{2+}-dependent endocytosis. *J. Cell Biol.* **2008**, *180*, 905−914.
(33) Rothenberger, S.; Iacopetta, B. J.; Kühn, L. C. Endocytosis of the transferrin receptor requires the cytoplasmic domain but not its phosphorylation site. *Cell* **1987**, *49*, 423−431.
(34) Kannan, K.; Stewart, R. M.; Bounds, W.; Carlsson, S. R.; Fukuda, M.; Betzing, K. W.; Holcombe, R. F. Lysosome-associated membrane proteins h-LAMP1 (CD107a) and h-LAMP2 (CD107b) are activation-dependent cell surface glycoproteins in human peripheral blood mononuclear cells which mediate cell adhesion to vascular endothelium. *Cell Immunol.* **1996**, *171*, 10−19.
(35) Kagiya, G.; Ogawa, R.; Ito, S.; Fukuda, S.; Hatashita, M.; Tanaka, Y.; Yamamoto, K.; Kondo, T. Identification of a cis-acting element responsive to ultrasound in the 5′-flanking region of the human heme oxygenase-1 gene. *Ultrasound Med. Biol.* **2009**, *35*, 155−164.
(36) Un, K.; Kawakami, S.; Higuchi, Y.; Suzuki, R.; Maruyama, K.; Yamashita, F.; Hashida, M. Involvement of activated transcriptional process in efficient gene transfection using unmodified and mannose-modified bubble lipoplexes with ultrasound exposure. *J. Controlled Release* **2011**, *156*, 355−363.

Journal of Controlled Release 160 (2012) 362–366

Contents lists available at SciVerse ScienceDirect

Journal of Controlled Release

journal homepage: www.elsevier.com/locate/jconrel

Prophylactic immunization with Bubble liposomes and ultrasound-treated dendritic cells provided a four-fold decrease in the frequency of melanoma lung metastasis

Yusuke Oda [a,1], Ryo Suzuki [a,1], Shota Otake [a,1], Norihito Nishiie [a], Keiichi Hirata [a], Risa Koshima [a], Tetsuya Nomura [a], Naoki Utoguchi [a], Nobuki Kudo [b], Katsuro Tachibana [c], Kazuo Maruyama [a,*]

[a] Department of Biopharmaceutics, School of Pharmaceutical Sciences, Teikyo University, Japan
[b] Laboratory of Biomedical Engineering, Graduate School of Information Science and Technology, Hokkaido University, Japan
[c] Department of Anatomy, School of Medicine, Fukuoka University, Japan

ARTICLE INFO

Article history:
Received 15 July 2011
Accepted 6 December 2011
Available online 13 December 2011

Keywords:
Dendritic cells
Antigen delivery system
Cancer immunotherapy
Ultrasound
Liposomes

ABSTRACT

Melanoma has an early tendency to metastasize, and the majority of the resulting deaths are caused by metastatic melanoma. It is therefore important to develop effective therapies for metastasis. Dendritic cell (DC)-based cancer immunotherapy has been proposed as an effective therapeutic strategy for metastasis and recurrence due to prime tumor-specific cytotoxic T lymphocytes. In this therapy, it is important that DCs present peptides derived from tumor-associated antigens on MHC class I molecules. Previously, we developed an innovative approach capable of directly delivering exogenous antigens into the cytosol of DCs using perfluoropropane gas-entrapping liposomes (Bubble liposomes, BLs) and ultrasound. In the present study, we investigated the prevention of melanoma lung metastasis via DC-based immunotherapy. Specifically, antigens were extracted from melanoma cells and used to treat DCs by BL and ultrasound. Delivery into the DCs by this route did not require the endocytic pathway. The delivery efficiency was approximately 74.1%. DCs treated with melanoma-derived antigens were assessed for *in vivo* efficacy in a mouse model of lung metastasis. Prophylactic immunization with BL/ultrasound-treated DCs provided a four-fold decrease in the frequency of melanoma lung metastases. These *in vitro* and *in vivo* results demonstrate that the combination of BLs and ultrasound is a promising method for antigen delivery system into DCs.

1. Introduction

Melanoma is the most devastating form of skin cancer and represents a leading cause of cancer death. Relative to the tumor mass, melanomas have an early tendency to metastasize; indeed, the majority of melanoma deaths are caused by metastatic disease. As a result, the prognosis for melanoma is poor. In fact, the 5-year survival rate of patients with localized melanoma is up to 90%; in contrast, patients with metastasized melanoma have 5-year survival rates of only 20% [1,2]. Additionally, melanoma is usually resistant to standard chemotherapy, and the response rate for any single agent or combination of agents ranges from 5% to 45% [3,4]. Based on these data, there is a clear need to develop effective therapy for metastasized melanoma. There are various therapeutic methods for metastatic cancer, such as surgical treatment, chemotherapy, radiotherapy, and immunotherapy. Of these methods, immunotherapy may be the most promising because of the possibility of preventing systemic metastasis and recurrence in the long term [5–9].

Dendritic cells (DCs), which are unique antigen-presenting cells capable of priming naive T cells, have been used as vaccine carriers for cancer immunotherapy [6,10]. To induce an effective tumor-specific cytotoxic T-lymphocyte (CTL) response, DCs should abundantly present epitope peptides derived from tumor-associated antigens (TAAs) via major histocompatibility complex (MHC) class I molecules and MHC class II molecules [11]. In general, exogenous antigens (such as TAAs in DCs) are preferentially presented on MHC class II molecules [12,13]. On the other hand, the majority of peptides presented via the MHC class I molecules are generated from endogenously synthesized proteins that are degraded by the proteasome [12]. Therefore, in order to efficiently prime TAA-specific CTLs, it is necessary to develop a novel antigen delivery system that can induce MHC class I-restricted TAA presentation on DCs. Several researchers have studied antigen delivery tools based on the cross-presentation theory of exogenous antigens in DCs [14–19]. Proposed antigen delivery carriers have included liposomes [15,16], poly(γ-glutamic acid) nanoparticles [17], and cholesterol pullulan nanoparticles [18]. All of these carriers deliver the antigens into DCs via the endocytic pathway, inducing the leaking of exogenous antigens from the endosome into the cytosol. Finally, it is thought that the antigens leaked into the cytosol are

Abbreviations: BL, Bubble liposome; CTL, cytotoxic T-lymphocyte; DC, dendritic cell; FITC, fluorescein isothiocyanate; MHC, major histocompatibility complex; MW, molecular weight; PBS, phosphate-buffered saline; TAA, tumor-associated antigen; US, ultrasound.

* Corresponding author at: Department of Biopharmaceutics, School of Pharmaceutical Sciences, Teikyo University, 1091-1 Suwarashi, Midori-ku, Sagamihara, Kanagawa 252-5195, Japan. Tel.: +81 42 685 3722; fax: +81 42 685 3432.
E-mail address: maruyama@pharm.teikyo-u.ac.jp (K. Maruyama).

[1] These authors contributed equally to this work.

0168-3659/$ – see front matter.
doi:10.1016/j.jconrel.2011.12.003

presented on MHC class I molecules. As an alternative, we have sought to use an antigen delivery system that does not rely on the endocytic pathway.

Multiple papers have reported the use of microbubbles for ultrasound-mediated gene and drug delivery [20–26]. In this delivery system, microstreams and microjets, which are induced by disruption of nano/microbubbles exposed to ultrasound, promote the transfer of extracellular materials into cells by opening transient pores in the cell membrane [27,28]. Previously, we described ultrasound-mediated antigen delivery in DCs using Bubble liposomes (BLs) containing perfluoropropane, an ultrasound imaging gas [29]. Using this system, a model antigen (ovalbumin) could be delivered into the cytosol of DCs independent of the endocytic pathway. This technique provided direct entry of the exogenous antigens into the MHC class I presentation pathway, resulting in the priming of exogenous antigen-specific CTLs. We proposed that this system could facilitate the delivery of crude antigens (such as tumor lysates and extracts) because such substrates could enter cells via a transient pore. In the present study, we used fluorescein isothiocyanate (FITC)-dextran as a substrate to characterize antigen delivery by BLs and ultrasound. Additionally, we assessed the possible application of BLs and ultrasound in DC-based immunotherapy in an *in vivo* model of melanoma. Specifically, we delivered tumor-extracted antigens into DCs using BLs and ultrasound, and investigated whether these treated DCs protected mice from lung metastasis.

2. Materials and methods

2.1. Cells

B16/BL6 cells, a C57BL/6-derived melanoma cell line, were cultured in RPMI 1640 (Sigma Co., St. Louis, MO, USA) supplemented with 10% heat inactivated fetal bovine serum (FBS, GIBCO, Invitrogen Co., Carlsbad, CA, USA), 50 U/ml penicillin, and 50 μg/ml streptomycin (Wako Pure Chemical Industries, Osaka, Japan).

2.2. Generation of mouse bone marrow-derived DCs

DCs were generated from bone marrow cells, as described elsewhere [30]. Briefly, bone marrow cells were isolated from C57BL/6 mice and were cultured in RPMI 1640 supplemented with 10% FBS, 50 μM 2-mercaptoethanol (Sigma Co., St. Louis, MO, USA), 50 U/ml penicillin, 50 μg/ml streptomycin, and 40 ng/ml mouse granulocyte-macrophage colony-stimulating factor (GM-CSF, PeproTech Inc., Rocky Hill, NJ, USA). After 8–16 days of culture, non-adherent cells were collected and used as DCs.

2.3. Preparation of BLs

Liposomes composed of 1,2-distearoyl-sn-glycero-phosphatidylcholine (DSPC) (NOF Co., Tokyo, Japan) and 1,2-distearoyl-sn-glycero-3-phosphatidyl-ethanolamine-methoxypolyethyleneglycol (DSPE-PEG (2 k)-OMe (NOF Co.)), 94:6 (mol:mol), were prepared by reverse phase evaporation. BLs were prepared from the liposomes and perfluoropropane (Takachiho Chemical Industrial Co., Ltd., Tokyo, Japan) as reported before [31,32]. Briefly, 5-ml sterilized vials containing 2 ml of the liposome suspension (lipid concentration: 2 mg/ml) were filled with perfluoropropane, capped, and then supercharged with 7.5 ml of perfluoropropane. The vials were placed in a bath-type sonicator (42 kHz, 100 W; BRANSONIC 2510J-DTH, Branson Ultrasonics Co., Danbury, CT, USA) for 5 min to form the BLs. In this method, the liposomes were reconstituted by sonication under the condition of supercharge with perfluoropropane in the 5-ml vial container. At the same time, perfluoropropane would be entrapped within lipids as micelles (composed of DSPC and DSPE-PEG(2k)-OMe), so forming nanobubbles. The lipid nanobubbles were encapsulated within the reconstituted liposomes, the sizes of which were increased from ~150–200 nm to ~500 nm.

2.4. Extraction of antigens from B16/BL6 cells

The extraction of antigens from B16BL/6 cells was performed by a butanol extraction method [33]. B16/BL6 cells were washed twice with phosphate-buffered saline (PBS) and then incubated with PBS containing 2.5% (v/v) 1-butanol. The solution was collected and centrifuged twice at 1600 ×*g* at 4 °C. The supernatant was dialyzed with water using a Spectra/Por Dialysis Membrane (MWCO: 10,000; Spectrum Laboratories, Inc., Rancho Dominguez, CA, USA). The dialysate then was centrifuged at 1600 ×*g* at 4 °C, and the resulting supernatant was freeze-dried.

2.5. FITC-dextran or B16/BL6-extracted antigen delivery following inhibition of the endocytic pathway in DCs

B16/BL6-extracted antigens were labeled with Alexa Fluor 633 Succinimidyl Esters (Invitrogen Co., Carlsbad, CA, USA) (Alexa-B16/BL6). DCs were pretreated with OptiMEM (Invitrogen Co.) containing 10 mM NaN_3 for 1 h at 4 °C to inhibit the endocytic pathway [34,35]. After washing the cells, BLs (120 μg) and FITC-dextran (Sigma Co.) or Alexa-B16/BL6 were added to the DCs in OptiMEM containing 10 mM NaN_3. The DCs were exposed to ultrasound (frequency: 2 MHz, duty: 10%, burst rate: 2.0 Hz, intensity 2.0 W/cm^2, time: 3 × 10 s (interval: 10 s)) using a Sonopore 4000 (6-mm diameter probe; Nepa Gene Co. Ltd., Chiba, Japan), then washed with PBS containing 10 mM NaN_3. The delivery efficiency of FITC-dextran or Alexa-B16/BL6 delivery was analyzed by flow cytometry [36].

2.6. Immunization with antigen-loaded DCs following BLs and ultrasound

DCs (2.5×10^5 cells) were pulsed with antigens (50 μg) exposed to ultrasound and/or BLs (120 μg) in a 48-well plate; the contents of 10 wells then were collected, pooled, and seeded into 1 well of a 6-well plate. After 1 h of incubation at 37 °C, the DCs were washed with medium and cultured for 24 h at 37 °C. The cells were washed with PBS, and the DCs (1×10^6 cells/100 μl) then were injected intradermally into the backs of C57BL/6 mice twice with a one-week interval.

2.7. B16/BL6 experimental lung metastasis model

C57BL/6 mice were immunized twice with DCs as described above. Seven days after the second immunization, B16/BL6 cells (1×10^5 cells/100 μl) were injected into the tail vein. The mice were sacrificed two weeks after the tumor cell injection, and the lungs were harvested and fixed in neutral buffered formalin (10%). The number of B16/BL6 colonies present on the surface of each set of lungs was determined by visual inspection using a stereoscopic dissecting microscope [37].

2.8. Statistical analysis

Differences in the number of lung metastatic colonies between the experimental groups were compared using non-repeated measures analysis of variance (ANOVA) with post-hoc Dunnett's test.

3. Results

3.1. FITC-dextran delivery into DCs by BLs and ultrasound

In BL/ultrasound antigen delivery, extracellular antigens are delivered into cells via the formation of transient membrane pores. Therefore, this technique is expected to deliver antigens into DCs as a function of both

pore size and molecular substrate size. In the present study, we used various molecular weight (MW) FITC-dextran molecules as model antigens and assessed the delivery efficiency of FITC-dextran into DCs. (Fig. 1(a–c)). In DCs treated with FITC-dextran (MW 4000) alone, the mean fluorescence intensity was 4-fold higher than non-treated DCs (Fig. 1(a)). On the other hand, upon treatment with FITC-dextran, BLs, and ultrasound, the mean fluorescence intensity was 2-fold higher than that with FITC-dextran alone. We also observed similar phenomena upon treatment with other sizes of FITC-dextran (MW 20,000 and 70,000) (Fig. 1(b), (c)). In addition, to assess the effect of molecular size on delivery efficiency, the fluorescence intensity was compared among FITC-dextrans (MW 4000, 20,000 and 70,000) delivered with BLs and ultrasound (Fig. 1(d)). The percentages of FITC-positive cells (M1 gated) were not affected by molecular weight, determined as 86.0% (MW: 4000), 87.3% (MW: 20,000), and 77.4% (MW: 70,000). On the other hand, the fluorescence intensity decreased as the molecular weight increased. The mean of fluorescence intensities were 24.5 (MW: 4000), 22.4 (MW: 20,000), and 16.5 (MW: 70,000).

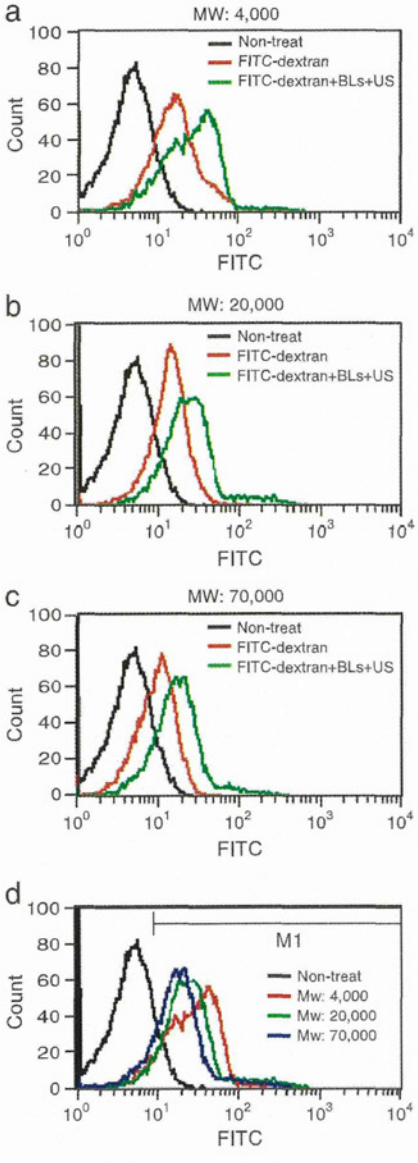

Fig. 1. Effect of molecular size on delivery into DCs using BLs and ultrasound. DCs were incubated with FITC-dextran, exposed to ultrasound in the presence of BLs, and washed with PBS. Delivery efficiency of FITC-dextran was analyzed using flow cytometry. Endocytosis by the DCs was inhibited by the inclusion of 10 mM sodium azide in all solutions and washes. Panels (a) to (c): Experiments were performed with FITC-dextran at a molecular weight of 4000, 20,000, or 70,000, respectively. Panel (d): Molecular weight dependency was analyzed following treatment with the combination of BLs and ultrasound. The percentages of M1 gated cell were quantified as follow: MW: 4000: 86.0%, MW: 20,000: 87.3%, MW: 70,000: 77.4%. The mean of fluorescent intensities were quantified as follow: MW: 4000: 24.5, MW: 20,000: 22.4, MW: 70,000: 16.5.

3.2. B16/BL6-extracted antigen delivery into DCs by BLs and ultrasound

Having demonstrated that the combination of BLs and ultrasound could deliver extracellular molecules of varying sizes, we sought to demonstrate that antigens extracted from B16/BL6 cells could be delivered into DCs by the same technique. Therefore, we assessed the delivery efficiency using Alexa Fluor 633-labeled antigens derived from B16/BL6 cells (Alexa-B16/BL6). As shown in Fig. 2, the DCs treated with antigens or the DCs treated with antigens and either BLs or ultrasound had fluorescence intensity profiles similar to those of untreated DCs. Flow cytometry confirmed this resemblance, with the percentages of Alexa-B16/BL6-positive cells (M2 gated) determined as 5.7% (antigen only), 6.5% (antigen and BLs), and 7.3% (antigen and ultrasound). In contrast, DCs treated with the combination of all three factors (antigens, BLs, and ultrasound) had an elevated fluorescence intensity profile compared with the other groups. Flow cytometry revealed that the percentage of Alexa-B16/BL6-positive cells was 74.1%.

3.3. Reduction in B16/BL6 lung metastasis following immunization with treated DCs

We employed an *in vivo* B16/BL6 experimental lung metastasis model to determine the anti-metastasis efficacy of DCs treated with tumor antigens delivered using BLs and ultrasound. C57BL/6 mice were immunized twice with bone marrow-derived DCs that were either untreated (no antigen exposure) or into which antigens had been delivered by one of four regimens (antigen alone; antigen + BLs; antigen + ultrasound; or antigen + BLs + ultrasound). As shown in Fig. 3(a), immunization with DCs that had been exposed to no antigen, antigen alone, or antigen with BLs *or* ultrasound weakly suppressed tumor metastasis. In contrast, immunization with DCs that had been exposed to antigens delivered via BLs *and* ultrasound reduced lung metastases four-fold, a decrease that was statistically significant ($P<0.05$) compared to the other groups. These numbers were consistent with the results of macroscopic inspection of lungs from the mice by stereoscopic microscopy, as shown in Fig. 3(b).

4. Discussion

The combination of ultrasound and microbubbles/nanobubbles has been reported to be an effective non-viral gene delivery method

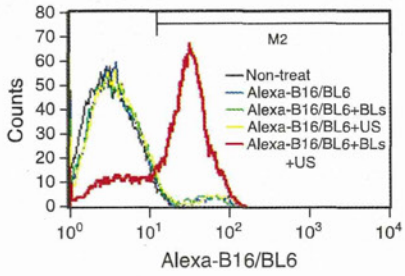

Fig. 2. Intracellular Alexa-B16/BL6 delivery into DCs using BLs and ultrasound. DCs were incubated with Alexa-labeled B16/BL6 extract, exposed (as indicated) to ultrasound and/or BLs, and washed with PBS. Delivery efficiency of Alexa-B16/BL6 was analyzed using flow cytometry. Endocytosis by the DCs was inhibited by the inclusion of 10 mM sodium azide in all solutions and washes. The percentages of M2 gated cell were quantified as follows: Alexa-B16/BL6: 5.7%; Alexa-B16/BL6 + BLs: 6.5%; Alexa-B16/BL6 + ultrasound 7.3%; Alexa-B16/BL6 + BLs + ultrasound: 74.1%.

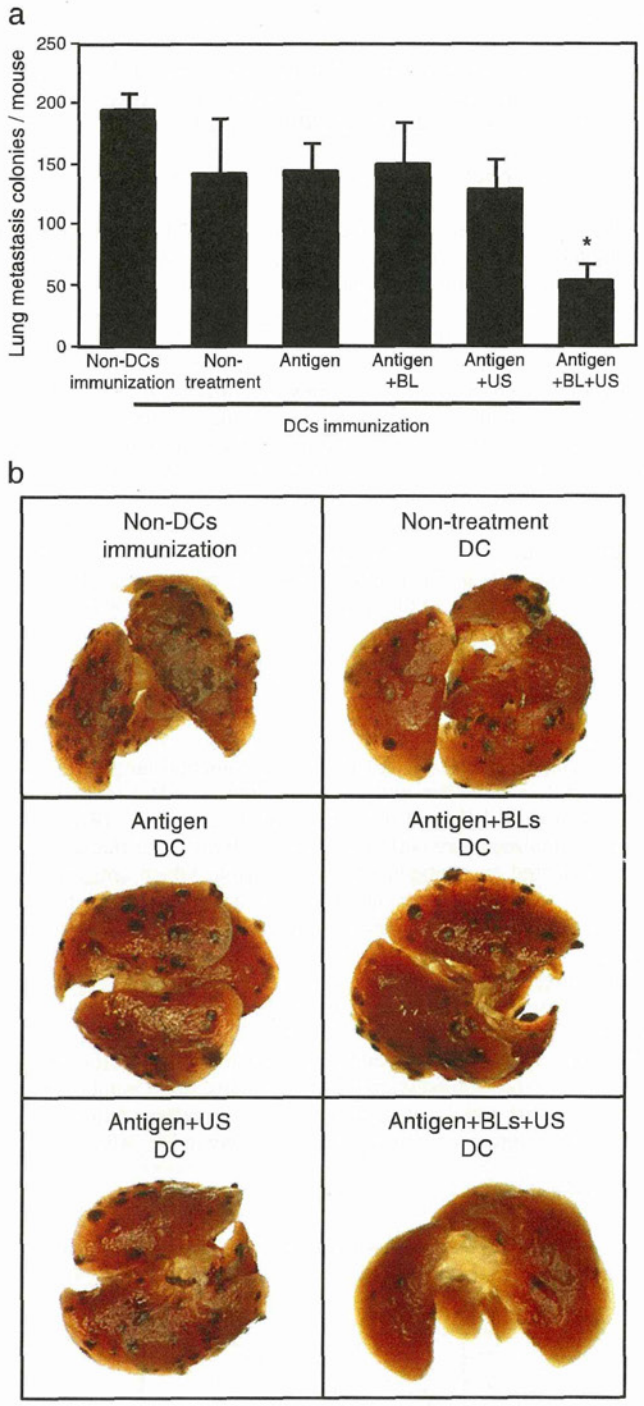

Fig. 3. Reduction of B16/BL6 lung metastasis following immunization with B16/BL6-treated DCs. DCs were treated with B16/BL6-extracted antigens and cultured as described in Materials and methods. C57BL/6 mice were immunized with the DCs twice with a one-week interval. One week after the second immunization, B16/BL6 cells were injected into the tail vein; after another two weeks, animals were sacrificed and lungs assessed for metastases. (a) Counts of lung metastatic colonies (means ± SDs; n = 6). *P < 0.05 (ANOVA, comparing all DC-immunized groups). (b) Images of lung by stereomicroscope.

for whole cells. This technique also has been applied for peptide and protein delivery [38–40]. In a previous study, we proposed the use of this technique for the delivery of novel antigens into DCs for cancer immunotherapy [29]. Entry into cells is believed to reflect the presence of transient pores in the cell membrane, permitting extracellular molecules direct access to the cytosol [21,28,41]. The present study confirmed that antigen was delivered into DCs by the combination of BLs and ultrasound, with delivery observed despite inhibition of the endocytic pathway. Thus, BLs appear to play a role similar to that of microbubbles for ultrasound-mediated substrate delivery. The present study also demonstrated an inverse correlation between the size of the substrate (MW of FITC-dextran) and the efficiency of delivery (fluorescence intensity). These results are consistent with a dependence of antigen delivery on pore size, which in turn depends on the degree of sonoporated cell membranes by BLs. The effect of pore size is expected to limit the delivery of larger molecules. However, this effect should not prevent the application of BL/ultrasound methods for antigen delivery, given that we were able to demonstrate the immunotherapeutic potential of the technique in an *in vivo* mouse model of lung cancer metastasis. As shown in the present work, we still observed delivery (albeit at a reduced level) even for a molecule (FITC-dextran) with a MW of 70,000. FITC-dextran is a bulky polymer with a straight chain; by comparison, most proteins are tightly packed, with a resulting decrease in apparent size. Therefore, various antigens of a range of sizes should still be able to be delivered into DCs using the BL/ultrasound delivery system.

Melanoma is generally considered a highly immunogenic cancer, and several melanoma-associated antigens (e.g., MAGE, MART-1, gp-100) have been identified [8,42]. However, we thought that it was important to establish an antigen delivery system that was suitable for various extracts containing unknown TAAs, since such a technique would be applicable for the induction of a variety of CTL clones [6]. In the present study, we tested BL/ultrasound delivery with TAAs obtained (via butanol extraction) from B16/BL6 cells. The use of butanol extraction is especially appealing because this method has been shown to solubilize a subset of hydrophobic proteins [33] that would presumably include various known and novel TAAs. Antigens delivered to the cytosol of DCs are expected to induce MHC class I presentation by these DCs, in turn inducing antigen-specific CTLs [12]. In the present work, the utility of BL/ultrasound delivery of a crude extract was demonstrated for the B16/BL6 antigens both *in vitro* (Fig. 2) and *in vivo* (Fig. 3).

The *in vivo* assay described here tested the efficacy of B16/BL6 antigens in reducing lung metastasis. Specifically, DCs were exposed to antigens in the presence of BLs and ultrasound, and the treated cells were used for prophylactic immunization of mice. Immunization significantly decreased lung metastasis, indicating that the treated DCs induced a B16/BL6-specific anti-tumor immune response. Given the poor prognosis seen with metastases [3,4], and the challenge of preventing systemic metastasis in the long term, such a therapeutic strategy for metastatic cancer is desperately needed. From this perspective, DC-based cancer immunotherapy is an attractive option: this approach should induce systemic and specific immune responses via antigen presentation, and while also controlling metastasis and recurrence in the longer term via immunological memory [6]. Matheoud et al. reported that immunization of DCs has a potency to reduce the metastasis in therapeutic model (by post-immunization) [43]. To induce more effective immune responses, we are optimizing about antigen delivery for DCs by BLs/ultrasound. After optimization, we will attempt to prevent metastasis in therapeutic model. The combination of BLs and ultrasound is expected to induce effective immune response in DC-based cancer immunotherapy by delivering various TAAs into DCs for potential clinical applications.

Acknowledgments

The authors thank Mr. Eisuke Namai, Mr. Yasuyuki Shiono, Mr. Ken Osawa, Ms. Motoka Kawamura, Mr. Ryo Tanakadate, Mr. Kunihiko Matsuo, Mr. Yudai Kawashima, Mr. Hitoshi Uruga, and Ms. Mutsumi Seki (Teikyo University) for their technical assistance,